Geochronology, mineral chemistry and paragenesis of REE mineralization in alkaline rocks from the Kohistan Island Arc, Pakistan

Amjad Hussain [a], Kui-Dong Zhao [a]*, Muhammad Arif [b, c], Martin R. Palmer [d], Qiang Zhang [a], Qian Li [a], Shao-Yong Jiang [a], Wei Chen [a], Musa Bala Girei [a]

[a] *State Key Laboratory of Geological Processes and Mineral Resources, Collaborative Innovation Center for Exploration of Strategic Mineral Resources, School of Earth Resources, China University of Geosciences, Wuhan 430074, PR China*

[b] *Department of Earth Sciences, Abbottabad University of Science and Technology, Havelian (Abbottabad), Pakistan*

[c] *Department of Geology, University of Peshawar, Pakistan*

[d] *School of Ocean and Earth Science, University of Southampton, Southampton SO14 3ZH, UK*

*****Corresponding author, E-mail address: zhaokd@cug.edu.cn (K.-D. Zhao)

Abstract

Alkaline igneous-related rare earth element (REE) deposits constitute a major global economic resource of REE. However, our understanding of their geodynamic settings and magmatic-hydrothermal processes remains uncertain. Here, we present an investigation of petrography, geochronology and mineral chemistry of newly discovered REE mineralization in the alkaline syenite and pegmatite from the Kohistan Batholith in the Kohistan Island Arc, Pakistan. The pegmatite contains abundant chevkinite and monazite (up to 10–35% in volume), which formed from crystallization of a REE-oversaturated evolved melt and are the main REE-bearing phases. UTh-Pb isotopic dating of zircon from the syenite yields the emplacement age of 31.2 ± 0.3 Ma, which closely matches the ages of zircon and monazite from the pegmatite (30.1 ± 0.3 Ma and 30.9 ± 0.3 Ma, respectively). Zircons from the syenite and the pegmatite have similar εHf(t) values, ranging from + 0.2 to + 2.5, indicating that the syenite and the pegmatite are co-magmatic in origin. The alkaline magma likely formed by partial melting of the enriched lithospheric mantle induced by the asthenospheric upwelling, which was related to slab break-off at the post-collisional stage following the collision of the Kohistan Island Arc with the Indian Plate. Zircons show the evolutional trend in trace element compositions from the syenite to the pegmatite, marked by increases in REE, Hf, Y, U, volatiles and fO_2. These changes reflect prolonged fractional crystallization processes of the alkaline magma, which were responsible for the REE enrichment in the residual pegmatitic melt. Postcollisional alkaline magmatic rocks are widely distributed in many places along the Tethyan orogenic belt. These observations

suggest that these post-collisional alkaline rocks may be good targets for REE exploration.

Keywords: REE mineralization, syenite, pegmatite, Kohistan Island Arc, Pakistan

1. Introduction

The majority of economic deposits of rare earth elements (REE) are hosted by: (1) carbonatites, (2) silica-deficient peralkaline rocks, (3) peralkaline granites and pegmatites, (4) granitic pegmatites and (5) iron oxide-phosphate deposits (Chakhmouradian and Zaitsev, 2012). Hence, REE deposits are predominantly associated with intracontinental, anorogenic, rift-related extensional settings formed by pull-apart tectonics and/or the asthenospheric upwelling (Chakhmouradian and Zaitsev, 2012). Despite some experimental, fluid inclusion and isotopic studies, the mechanisms of fractionation, transportation and precipitation of REE to form economically important deposits in alkaline rocks are not fully understood (e.g. Dostal, 2017; Siegel et al., 2018). Most models suggest that REE enrichment in alkaline rocks is related to halogen-mediated magmatic processes which culminate the formation of an immiscible REE-rich fluoride melt and a silicate melt (e.g. Veksler et al., 2005). Previous investigations suggest that extensive fractional crystallization plays the dominant role for hyper-enrichment of REE and other critical metals in alkaline rocks, especially in their highly evolved lithologies (e.g. pegmatites) (Dostal, 2016; Kempe et al., 1999). However, it has also been shown that hydrothermal fluids can mobilize REE as F^-, Cl^-, CO_3^{2-}, and OH^- complexes that can concentrate the REE in veins (e.g. Williams-Jones et al., 2012). Thus, there is a general consensus that both magmatic and hydrothermal processes play significant roles in the formation of REE deposits in alkaline rocks and carbonatites (Dostal et al., 2014; Siegel et al., 2018; Tillberg et al., 2019; Ying et al., 2020).

The principal focus of this study is the newly discovered REE mineralization in the alkaline rocks within the Tangir-Darel area of northern Pakistan (Fig. 1). Abundant REE minerals are hosted in the pegmatite that is intimately associated with the syenite in the Kohistan Batholith in the Kohistan Island Arc (KIA) system. Liziero (2008) presented a preliminary report on the REE-mineral chevkinite from this area, whereas the genetically details regarding the mineralization are lacking. Here, we present geological details, petrography, mineralogy, geochemistry and U-Th-Pb geochronological data for the syenite and the mineralized pegmatite, aiming to understand the timing and formation conditions of REE mineralization. In addition, the tectonic environment for the alkaline magmatism within the Kohistan Island Arc is discussed.

2. Geological setting

The Kohistan Island Arc (KIA) in northern Pakistan is one of the world's best examples of an intra-oceanic island arc, displaying a complete section through the arc's lowermost crustal and subjacent mantle sections of ultramafic–mafic rocks, then to supra-crustal cover (e.g. volcanic and sedimentary rocks) (Fig. 1a) (Petterson, 2010). The KIA initiated through intra-oceanic subduction and largely grew within an intra-oceanic setting. Then it was sutured to the southern margin (the Karakoram microplate) of the Eurasian plate along the Main Karakoram Thrust (MKT) or the Shyok suture at ~ 75–102 Ma, and thrusted on to the north-western part of the Indian plate along the Main Mantle Thrust (MMT) or the Indus suture at ~ 45–50 Ma (Fig. 1a) (Molnar and

92 Tapponnier, 1975; Petterson and Windley, 1985; Rehman et al., 2011; Treloar et al.,
93 1989). Suturing to the Eurasian plate changed the KIA to an Andean-type margin, with
94 magmatism in the KIA system continuing during and after suturing.

95 In addition to variably metamorphosed and mineralogically diverse volcanic
96 and sedimentary lithologies, the KIA contains three plutonic rock sections; the Southern
97 Plutonic Complex, the Chilas Complex, and the Kohistan Batholith (Fig. 1a). The
98 ultramafic–mafic rocks of the Jijal and Spat complexes and amphibolite facies rocks of
99 the Kamila Belt, representing the KIA's upper mantle and lower-middle crustal parts,
100 respectively, collectively make up the Southern Plutonic Complex (Burg et al., 2005).
101 The Chilas Complex is a huge diapiric mafic intrusion emplaced during intra-arc to
102 back-arc rifting at 80–85 Ma (Jagoutz et al., 2007; Khan, 1989). This complex consists
103 of abundant gabbronorite, diorite, and quartz diorite, locally present subordinate dunite,
104 peridotite and pyroxenite, and minor troctolite and anorthosite.

105 The Kohistan Batholith (KB) is one of the major units of the KIA and consists
106 of numerous isolated plutons, dykes, and sills of calc-alkaline gabbroic to leucogranitic
107 composition. Petterson and Windley (1985) recognized three main intrusion stages
108 within the Kohistan Batholith based on differences in ages and the presence or absence
109 of gneissic fabric in the constituent granitoids. Following this subdivision, Jagoutz et
110 al. (2018) suggested that the stage 1 rocks are predominantly deformed, subduction-
111 related, and composed of gabbro, diorite, and tonalite. The stage 2 rocks are Andean-
112 type plutons, including the 85–40 Ma diorite, granite, and leucogranite. The stage 3

113 rocks are represented by aplite-pegmatite bodies (or dykes) with ages mostly ranging
114 from 34 to 26 Ma.

115 The alkaline rocks (the syenite and the pegmatite) in this study lie at the
116 southern part of the Kohistan Batholith in the upper reaches of Tangir and Darel Nala
117 (Fig. 1b). The Kohistan Batholith in this area consists exclusively of granite, syenite
118 and pegmatite, representing the stage 3 rocks, which intruded into the gabbronorite and
119 diorite of the Chilas Complex. The syenite hosts variously shaped patches and dykes of
120 pegmatite (Fig. 2a–f), which contain abundant REE-bearing phases including
121 chevkinite, monazite and apatite of potential economic significance.

122

123 **3. Petrography**

124 *3.1. Syenite*

125 The syenite exhibits porphyritic texture (Fig. 2a) and consists of abundant alkali
126 feldspars (perthite and orthoclase), with subordinate aegirine and richterite, and
127 accessory amounts of biotite, monazite, apatite, chevkinite, zircon, titanite and quartz.
128 The mafic and felsic phases are generally distributed homogeneously, but some mafic
129 minerals (e.g. aegirine) are segregated into clusters in places (Fig. 3a). The alkali
130 feldspars (perthite and orthoclase) are the most abundant minerals with modal
131 proportions ranging from 60 to 70 vol% and grain sizes of 1.5–3.0 mm. The perthite
132 grains display exsolution of albite in the form of lamellae and irregularly shaped blebs.
133 The plagioclase grains are evenly distributed (Fig. 3b) and their modal abundances are

5–10 vol%. Most of the feldspar crystals are euhedral, while mafic minerals are anhedral to subhedral interstitial to feldspars (Fig. 3a–d), which suggests that mafic minerals crystallized later than felsic minerals. Aegirine is the next most abundant phase after perthite with model proportions of 15–20 vol%. Most of the aegirine grains are interstitial to early-formed felsic minerals (Fig. 3a), and some euhedral aegirine grains are partially or fully enclosed by felsic minerals (Fig. 3b). Richterite, a sodic-calcic amphibole, is also present in the syenite, with modal proportions (< 3 vol%) less than those of aegirine (Fig. 3c).

The syenite contains miaskitic-like accessory minerals (e.g. zircon, titanite, and other Ti-bearing phases) rather than agpaitic accessory minerals (e.g. halogen-bearing Na-Ca-HFSE phases) (Marks and Markl, 2017). Chevkinite occurs as medium- to large-sized, subhedral to anhedral discrete grains mostly in the interstices of the felsic and mafic minerals (Fig. 3d). Medium- to large-sized euhedral monazite is common in the syenite and occurs mostly in the form of cluster (Fig. 3e). The 30–150 μm wide and 50–600 μm long grains of monazite show a cross-cutting relationship with the mafic minerals (Fig. 3f). The presence of tiny inclusions of aegirine within monazite grains also indicates a relatively later crystallization of monazite (Fig. 3a). Apatite occurs as medium- to large-sized, euhedral to subhedral grains (Fig. 3g). The apatite grains display cross-cutting relationships with the mafic minerals (Fig. 3h), which suggests relatively later crystallization compared to aegirine. Discrete anhedral to subhedral, medium-sized grains of zircon and titanite occur in trace amounts. Trace amounts of fine- to coarse-grained calcite also occur in a few samples (Fig. 3i), especially in

156 samples from the contact zone between the syenite and the pegmatite. The calcite grains
157 are mostly embedded in the aegirine sheaves, suggesting that calcite precipitation was
158 triggered by an increase of volatile contents in the later magma. Accessory amounts of
159 very fine-grained quartz (< 2 vol%) occur in the spaces of other felsic mineral grains.

160 *3.2. Pegmatite*

161 Pegmatitic rocks commonly occur as randomly oriented dykes, veins and small
162 lenticular patches in the syenite (Fig. 2b–f). The width of the pegmatitic dykes varies
163 from 3 to 70 cm, and their length ranges from decimeter up to 1 m. The pegmatitic
164 dykes do not display discernible zonation and show irregular, but sharp, contact with
165 the enclosing syenite (Fig. 2b–f). The overall texture of the pegmatite is allotriomorphic
166 and is characterized by heterogeneous mineral distribution with highly variable grain
167 sizes. The pegmatite contains abundant perthite, richterite, aegirine, chevkinite,
168 monazite (Fig. 2g–i), and trace amounts of apatite, thorite, titanite, zircon, barite, calcite
169 and fergusonite. The distinctly larger grain size of perthite compared to other minerals
170 gives the pegmatite a megaporphyritic texture (Fig. 2d–g and Fig. 4a). Abundant
171 richterite and aegirine (20–30 vol%) occur as large to mega-grained euhedral crystals
172 (Fig. 4b–d). The pegmatite contains abundant chevkinite (5–15 vol%), which is one of
173 the main REE-bearing minerals. Chevkinite occurs as mega-grained crystals (Fig. 2b–
174 h) and inclusions within richterite, aegirine and perthite (Fig. 4e,f), suggesting that
175 chevkinite crystallized together with or earlier than mafic phases. The crystallization of
176 chevkinite may have commenced at the onset of the pegmatitic stage, i.e. immediately
177 after the syenitic stage (Fig. 5). The modal proportions of monazite in the syenite do

not exceed trace amounts, but are markedly higher (up to 10–20 vol%) in the pegmatite. Monazite occurs as euhedral to subhedral grains that are widely dispersed as both discrete crystals and clusters (Fig. 4f–h). Monazite also occurs as inclusions in the felsic and mafic silicate minerals and can be found in the interstices between large chevkinite grains.

Trace amounts of medium to coarse-grained zircon occur in the pegmatite (Fig. 4i). Textural observations suggest that zircon crystallized earlier than monazite, titanite, and most other phases except chevkinite. Very thin veins and discrete grains of calcite are common in the pegmatite (Fig. 4b,c). Anhedral grains of thorite and barite are present in trace amounts. The irregular form and intimate association of thorite and chevkinite suggest that thorite may have formed at the expense of chevkinite. In spite of drastically different in terms of grain sizes and modal compositions, the pegmatite and syenite contain qualitatively similar rock-forming and REE-rich minerals (Fig. 5), suggesting a strong genetic link between the two. The crystallization fractionation of alkali feldspar and plagioclase from the syenitic melt might cause the enrichment of REE and volatiles in the residual pegmatitic melt.

4. Analytical methods

4.1. LA-ICP-MS U-Pb dating and trace element analyses of zircon

Zircon grains from the syenite samples were separated using a conventional heavy liquid and magnetic separation technique. The zircon grains were handpicked under a binocular microscope, mounted in epoxy and polished. Cathodoluminescence (CL) images of the zircons were taken to observe the internal structure and morphology.

U-Th-Pb isotopic dating and trace element analyses of zircon were carried out by LA-ICP-MS at the State Key Laboratory of Geological Processes and Mineral Resources (GPMR), China University of Geosciences, Wuhan. Laser ablation was coupled with a RESOlution S-155 193 nm ArF excimer laser and the ablation protocol employed a spot diameter of 33 μm at a 10 Hz repetition rate. Helium was used as the carrier gas and argon was used as the make-up gas. A small amount of nitrogen was added to the main gas flow to increase sensitivity (Hu et al., 2008). The carrier and make-up gas flows were optimized by ablating NIST 612 glass to obtain maximum signal intensity for ^{238}U and close to one for the $^{238}U/^{232}Th$ ratios. NIST 610 glass (Gunther and Hattendorf, 2005) was used as a bracketing standard to correct for instrumental drift. Zircon 91,500 (Wiedenbeck et al., 1995) was used as an external standard during isotopic analyses. Each analysis integrated background acquisition of 30 s gas blank followed by 40 s data acquisition. Quantitative calibrations for U-Th-Pb ages and trace elements of zircon were processed by ICPMSDataCal software (Liu et al., 2010, 2008). The weighted mean ages and Concordia diagrams were generated using the ISOPLOT/EX 3.23 software package (Ludwig, 2003).

4.2. LA-ICP-MS U-Pb dating of monazite

U-Th-Pb dating of monazite in thin sections from the pegmatite samples was conducted by an Agilent 7900 ICP-MS equipped with a GeolasPro laser ablation system at the Sample Solution Analytical Technology Co. Ltd., Wuhan, China. The spot size and frequency of the laser were 16 μm and 2 Hz, respectively. Monazite from the Trebilcock

221 pegmatites (272 ± 4 Ma) (Tomascak et al., 1996) was used as an external standard.
222 Analytical results were calculated using ICPMSDataCal software and diagrams were
223 generated using the ISOPLOT/EX 3.23 software package.

224 *4.3. EMPA major element analyses of chevkinite and monazite*

225 Electron microprobe analysis (EMPA) of major elements in chevkinite and monazite
226 was performed using a JEOL JXA-8230 electron microprobe at the Testing Center of
227 Shandong Bureau, China Metallurgical Geology Bureau. Operating conditions of 15
228 kV acceleration voltage and 5 μm spot beam diameter were used. All the analytical data
229 were corrected by the ZAF (atomic number absorption, fluorescence) method. The
230 following standard were used for quantitative analyses: jadeite (Si), garnet (Al), olivine
231 (Fe), diopside (Ca), rhodonite (Mn), rutile (Ti), monazite (Ce, La, Th), celestite (Sr).

232 *4.4. LA-ICP-MS trace element analyses of chevkinite and monazite*

233 Trace elements contents of chevkinite and monazite were measured by LA-ICP-MS at
234 GPMR. The NIST 610 and 612 glasses and the USGS reference glasses (BCR-2G,
235 BHVO-2G and BIR-1G) were analyzed between every 8 samples. Both standards and
236 samples were ablated using 33 μm spot size, 8 Hz repetition rate. The NIST standards
237 were used for correcting the signal drift. External calibrations were performed using the
238 USGS reference glasses. Raw data reduction was performed offline using the
239 ICPMSDataCal software.

240 *4.5. LA-MC-ICP-MS Hf isotopic analyses of zircon*

241 In-situ Hf isotopes of zircon were measured using the same laser attached to a Nu
242 Plasma II MC-ICP-MS at GPMR. A stationary 50 μm diameter beam spot was used to

243 ablate the sample. Atomic masses of 172, 173, 175, 176, 177, 178, 179, 180 and 182
244 were measured simultaneously in a static-collection mode. In order to correct the
245 isobaric interferences of ^{176}Lu and ^{176}Yb on ^{176}Hf, a ^{176}Lu/^{175}Lu ratio of 0.02655 and a
246 ^{176}Yb/^{173}Yb ratio of 0.7965 were used (Chu et al., 2002). The ^{179}Hf/^{177}Hf ratio of 0.7325
247 was used as an exponential law. An inhouse zircon standard (Penglai) yielded a
248 weighted mean ^{176}Hf/^{177}Hf ratio of 0.282915 ± 0.000014 (2σ, n = 20) in this study,
249 which is consistent with the reference value of 0.282906 ± 0.0000010 (Li et al., 2010).
250 The εHf(t) values were calculated using the ^{176}Lu decay constant of 1.867×10^{-11} year^{-1}
251 (Soderlund et al., 2004) and chondritic present-day values of ^{176}Lu/^{177}Hf (0.0336) and
252 ^{176}Hf/^{177}Hf (0.282785) derived from Bouvier et al. (2008).

253 **5. Results**

254 *5.1. U-Th-Pb ages of zircon and monazite*

255 Zircon grains from the syenite samples are euhedral to subhedral, transparent, and show
256 multiple magmatic zoning with a variable diameter of 100–200 μm, and length to width
257 ratios of 1:1 to 2:1 (Fig. 6a). The U-Th-Pb data for zircon by LA-ICP-MS are listed in
258 Table 1 and syenite yielded U and Th contents of 425–3601 ppm and 37–3041 ppm,
259 respectively. The Th/U ratios are 0.09–1.18. The analyses yielded concordant or nearly
260 concordant U-Pb ages, with a weighted mean ^{206}Pb/^{238}U age of 31.2 ± 0.3 Ma (n = 20,
261 MSWD = 0.82) (Fig. 7a,b).

262 Zircons from the pegmatite occur as anhedral to subhedral crystals and show
263 complex zonations (Fig. 6b–d), and subtle magmatic zoning is also visible in the CL
264 and BSE images. Over 50 spot analyses were taken on the pegmatitic zircons in the thin

sections, but only 10 analyses yielded concordant U-Pb ages, giving a weighted mean $^{206}Pb/^{238}U$ age of 30.1 ± 0.3 Ma (n = 10, MSWD = 0.88) (Fig. 7c,d). Zircons from the pegmatite show higher U contents (910–10717 ppm) and lower Th/U ratios (0.04–0.59) than those from the syenite.

Euhedral to subhedral grains of monazite in the pegmatite exhibit clear magmatic sector zoning (Fig. 6e,f). The LA-ICP-MS U-Th-Pb data for monazite are listed in Table 2 and illustrated in Fig. 7e,f. The U-Pb isotope data on monazite define a well-constrained line on the Tera-Wasserburg diagram (Fig. 7e) and yield a lower intercept age of 29.8 ± 1.5 Ma (MSWD = 1.8). The monazite has high Th contents of 3755–9373 ppm, which gave a weighted average $^{208}Pb/^{232}Th$ age of 30.9 ± 0.3 Ma (n = 27, MSWD = 2.9) (Fig. 7f).

5.2. Zircon trace element compositions

The trace elemental compositions of zircons analyzed by LA-ICP-MS are listed in Table 3. The studied zircons from both the syenite and the pegmatite show HREE-enrichment patterns (Fig. 8a), which are similar as typical magmatic zircons. Zircons from the pegmatite generally show higher REE contents than those from the syenite (Fig. 8a). In the La versus (Sm/La)N and Y versus Hf/Y diagrams (Fig. 8b,c), most zircons from the syenite plot in the magmatic zircon field, while most of the zircons from the pegmatite plot in the transitional field between magmatic and hydrothermal zircons defined by Hoskin (2005).

Zircons from the pegmatite show higher Ce/Ce* anomalies (44.5–591) than those from the syenite (28.5–74.6) (Fig. 8d). The abundances of Ce^{4+}/Ce^{3+} and fO_2 of

zircons were calculated from the REE contents and whole-rock data based on the lattice-strain model (Li et al., 2019). The calculations yielded higher Ce^{4+}/Ce^{3+} values (585–6296) and higher oxygen fugacity ($\log fO_2$: −18.1 ~ −3.8) for the pegmatite compared to those for the syenite (42–557, −22.9 ~ −8.5, respectively) (Table 3).

The higher Hf and Yb contents and lower Ti contents in zircons from the pegmatite than those from the syenite suggest decreasing magma temperatures from the syenite to the pegmatite (Fig. 8e,f). The Ti-in-zircon crystallization temperatures were calculated using the formula proposed by Ferry and Watson (2007):

$$\log(\text{Ti-in-zircon ppm}) = (5.711 \pm 0.0072) - (4800 \pm 86)/T(^{o}K) - \log\alpha SiO_2 + \log\alpha TiO_2.$$

Here, αSiO_2 and αTiO_2 are the activities of SiO_2 and TiO_2, respectively. During normal crystallization, these activities increase with fractionation until they reach saturation (Claiborne et al., 2010). In this study, crystallization of abundant Ti-bearing phases (e.g., titanite and chevkinite) and a small amount of quartz in the interstices, allowed αSiO_2 and αTiO_2 to be held constant at 1.0 and 0.6, respectively. The calculated temperatures range from 626 °C to 700 °C for the syenite, and from 496 °C to 645 °C for the pegmatite (Table 3).

The relationship between Th/U vs. Yb/Gd ratios for zircons in both the syenite and the pegmatite shows an obvious difference, which is mainly related to fractionation of amphibole and Ti-bearing phases (Fig. 8g). Compared to zircons from the syenite, zircons from the pegmatite generally have higher U contents and lower Th/U ratios (Fig. 8h). The Nb and Ta contents in zircons from both the syenite and the pegmatite show positive correlations (Fig. 8i).

309 *5.3. Zircon Lu-Hf isotope*

310 Zircon Lu-Hf isotope compositions are listed in Table 4. Twenty spot analyses on
311 zircons from the syenite yield $^{176}Hf/^{177}Hf$ ratios in the range of 0.282758 to 0.282817.
312 The calculated εHf(t) values range from + 0.2 to + 2.3, and single stage model ages
313 vary from 610 Ma to 699 Ma (Fig. 9). Fourteen spot analyses on zircons from the
314 pegmatite yield $^{176}Hf/^{177}Hf$ ratios of 0.282760 to 0.282827. The calculated εHf(t) values
315 range from + 0.2 to + 2.5, and single stage model ages vary from 621 Ma to 736 Ma.

316 *5.4. Chevkinite and monazite geochemistry*

317 Chevkinite and monazite are the main REE phases in the pegmatite. Chevkinite occurs
318 as euhedral to tabular, strongly pleochroic (dark brownish to deep red) crystals (Figs. 2
319 and 4). Chevkinite displays clear sector zoning on the back-scattered electron (BSE)
320 images (Fig. 10a,b). The major and trace element compositions of chevkinite are listed
321 in Table 5. According to the classification of Macdonald and Belkin (2002), the
322 chemical compositions of the bright and dark zones identified in the BSE images both
323 plot in the chevkinite field with the bright zones characterized by lower Ca and Sr
324 abundances (Fig. 11a,b). The studied chevkinite samples are plotted in the field of the
325 oversaturated evolved rock types on the diagram proposed by Macdonald and Belkin
326 (2002) (Fig. 11c). The ΣREE + Y concentrations in chevkinite vary from 41.21 wt% to
327 45.49 wt%. Substitution within the chevkinite follows the general equality of $(Ca + Sr)_A$
328 $+ (Ti + Zr)_C = (REE + Y) + (M^{+2}, {}^{+3})_C$ (Fig. 11d). The chevkinite shows a strongly
329 LREE-enrichment pattern in the chondrite normalized REE diagram (Fig. 11e).

330 The monazite grains mostly occur in clusters interstitial to feldspars and
331 aegirines, and show crosscutting relationships to mafic minerals. In BSE images,
332 monazite shows clear sector zoning (Fig. 10c–e). The major and trace element
333 compositions of monazite are listed in Table 6. The ΣREE + Y concentrations in the
334 monazite vary from 67.10 wt% to 70.20 wt%. The monazite has unusually high sulfur
335 contents (up to 0.60–1.07 wt% SO_3), which enter the monazite structure together with
336 Th and Si, replacing P and REE (Fig. 11f–h). The monazite also shows a strongly
337 LREE-enrichment pattern in the chondrite normalized REE diagram (Fig. 11i).
338
339 **6. Discussion**
340 *6.1. Zircon trace elements and Hf isotope: Constrain on petrogenesis*
341 Hf isotopic and trace element compositions of zircon can provide information about the
342 source and crystallization temperature of magma (Belousova et al., 2005; Hoskin and
343 Schaltegger, 2003; Thomas et al., 2002). Although the pegmatitic zircons exhibit
344 complex textural features, the magmatic zoning and the typical REE patterns of
345 magmatic zircons confirm their magmatic origin (Fig. 8a) (Černy et al., 1985). Similar
346 U-Pb ages and εHf(t) values of zircons from both the syenite and the pegmatite indicate
347 that they are coeval and co-magmatic in origin (Figs. 7 and 9). Zircons from the syenite
348 and the pegmatite yield relatively low but positive εHf(t) values that range from + 0.2
349 to + 2.5. This indicates that the parental magma was derived from the lithospheric
350 mantle that had likely been previously enriched during subduction processes.

Changes in trace element compositions of zircon can provide useful insights into the magma evolution (Hoskin and Schaltegger, 2003; Uher and Černy, 1998; Wark and Miller, 1993). Zircons from the pegmatite have higher REE contents than those from the syenite (Fig. 8a), indicating that magma evolution from the syenite to the pegmatite was marked by increasing REE contents. Compared to those from the syenite, zircons from the pegmatite have higher contents of Hf and Y (Fig. 8c), suggesting that they crystallized from a highly evolved melt (Belousova et al., 2005; Černy et al., 2012; Hoskin et al., 2000). The contents of U and Th also vary considerably between zircons from the syenite and the pegmatite, with the latter having higher contents. Although both U and Th substitute for Zr in zircon structure, Th/U ratios tends to decrease during fractional crystallization. Indeed, Th/U versus Yb/Gd ratios shows a negative trend (Fig. 8g), which is consistent with a magma evolutionary trend marked by crystallization fractionation of amphibole and Ti-bearing phases (Lee et al., 2017). Variation in Nb and Ta contents of zircon also give important insights into the magmatic evolution. Early crystal fractionation of silicate minerals and ilmenite, leads to an increase in Nb-Ta contents and a decrease in Ti contents. Therefore, highly evolved melt usually has high Nb-Ta contents and low Ti contents (Breiter et al., 2006; Linnen and Keppler, 1997; Stepanov et al., 2014). Zircons from the pegmatite show higher Nb-Ta contents and lower Ti contents than those from the syenite (Fig. 8e and i), again indicating that the REE-mineralized pegmatite formed from a highly evolved melt.

6.2. Physico-chemical conditions for magma and REE mineralization

373 Trace element compositions of zircon also yield useful clues regarding the temperature
374 and redox conditions of the crystallizing perature (Watson et al., 2006; Watson and
375 Harrison, 2005). Zircons from the syenite have higher Ti contents than those from the
376 pegmatite. The calculated zircon saturation temperatures based on the thermometric
377 model of Watson et al. (2006), yield higher values (626–700 °C) for the syenitic magma
378 than those for the pegmatitic magma (496–645 °C) (Fig. 12a,b). The calculated
379 temperatures are lower than the typical formation temperatures of alkaline rocks (800–
380 1000 °C, Clemens et al., 1986), probably due to the presence of high volatile contents
381 in the magma (e.g. Černy and Ercit, 2005).

382 The magnitude of the Ce* and Eu* anomalies and the Ce^{4+}/Ce^{3+} ratios in zircons
383 mainly depends on the redox state of the magma (Ballard et al., 2002; Trail et al., 2012).
384 Under oxidized condition, Ce mainly occurs in Ce^{4+} state, which is preferentially
385 incorporated into zircon structure due to the closer size similarity between Ce^{4+} and
386 Zr^{4+}. Following the lattice-strain model of Li et al. (2019), Ce^{4+}/Ce^{3+} ratios and fO_2 of
387 the zircons were calculated using whole-rock trace element compositions as proxies for
388 the melt. The calculated Ce*, Ce^{4+}/Ce^{3+} and fO_2 yielded higher values for the pegmatite
389 than those for the syenite (Fig. 12c,d), indicating that REE mineralization in the
390 pegmatite occurred under more oxidizing conditions, in agreement with data from
391 similar deposits elsewhere (Dostal, 2017).

392 *6.3. Mechanism for REE enrichment*

393 Constraining magmatic-hydrothermal processes, such as fractional crystallization,
394 crustal contamination, magmatic redox conditions and role of halogens (e.g., F, Cl) and

395 other volatiles (e.g. S, CO_2), is essential for understanding the genesis of REE
396 mineralization (Dostal, 2017; Dostal et al., 2014). Textural relationships indicate that
397 aegirine and feldspar precipitated earlier than richterite and biotite in the syenite. The
398 fractional crystallization of these anhydrous silicate minerals can cause the increasing
399 of H_2O and volatiles in the residual melt (Siegel et al., 2018). The anomalously high S
400 contents in monazite and the presence of magmatic calcite (Fig. 4b,c) in the pegmatite
401 also indicate high volatile contents. This likely caused a reduction in magma viscosity
402 and solidus temperature, which could in turn favor extensive fractional crystallization
403 and further REE enrichment during evolution of the alkaline magma (Černy and Ercit,
404 2005). This hypothesis is supported by an increasing trend in the total REE contents in
405 zircon with decreasing temperature from the syenite to the pegmatite.

406 The primary REE-bearing phases in the pegmatite include chevkinite, monazite,
407 apatite and zircon. Experimental studies suggest that the solubility of these REE-
408 bearing phases usually increases with an increasing degree of alkalinity and oxygen
409 fugacity (Ferry and Watson, 2007; Harlov et al., 2011). The high alkalinity, as inferred
410 from the presence of alkaline pyroxene and amphibole, likely enhanced the retention of
411 REE in the melt during magmatic evolution. The decomposition of the dissolved water
412 in the pegmatitic magma will result in the release of oxygen and the increasing of
413 oxygen fugacity (London, 2018). The high oxygen fugacity, as indicated by high zircon
414 Ce^{4+}/Ce^{3+} ratios, may have also increased the solubility of REE-bearing phases and
415 favored their retention in the magma until the pegmatitic stage. It is noteworthy that
416 although chevkinite in the pegmatite shows patchy zonation (Fig. 10a,b), the chemical

differences between the zones are very subtle (Fig. 11a–e), suggesting that these zonations were caused by only minor changes in temperature and pressure during chevkinite growth (e.g. Macdonald et al., 2013; MacDonald and Belkin, 2002). Thus, prolonged fractional crystallization resulted in the increasing of REE, Hf, Yb, Y, U, volatiles and fo_2 from the syenitic to the pegmatitic melt. When the melt temperature decreased to 650 °C or lower, abundant chevkinite and monazite crystallized from the melt to form the REE mineralization.

6.4. Timing of alkaline magmatism and tectonic implications

Previous studies have demonstrated that the KIA terrane underwent two major collisional events at 75 to 102 Ma and 45 to 50 Ma. The earlier event involved collision between the Eurasian plate and the KIA, which transformed the arc into an Andean-type continental margin (Petterson and Windley, 1985; Treloar et al., 1989). The later 45 to 50 Ma event involved collision between the KIA arc and the Indian plate, and resulted in southward overthrusting of the KIA onto the Indian continental margin (Coward et al., 1986) along the Main Mantle Thrust (Fig. 1a). Chronological data from this study suggests that the alkaline magmatism in the KIA occurred at 30–31 Ma, indicating that the 45–50 Ma collisional event was accompanied by prolonged postcollisional magmatism. The low, but positive εHf(t) values (+0.2 to + 2.5) for the syenite and associated pegmatite indicate that the parent magma was derived from an enriched lithospheric mantle. It is likely that the lithospheric mantle in the KIA was metasomatised during the preceding subduction event (Fig. 13a). Subduction-induced metasomatized mantle is enriched in LREE as well as LILE, due to melting of recycled

continentally-derived sediments (e.g. Hou et al., 2015). Partial melting of such metasomatized lithospheric mantle and overlaying lower crust is likely to produce the REE-rich alkaline magma.

Alkaline rocks generally formed from extensional settings caused by pull-apart tectonics and/or asthenospheric upwelling (Chakhmouradian and Zaitsev, 2012). According to Burg (2011), the extensional features with exposure of extruded coesite-bearing rocks along the Main Mantle Thrust strongly suggest that the slab break-off was likely to occur in post-collisional settings in KIA around 45–25 Ma. The detail geophysical investigations of KIA also reveal that the propagation of large conductive mantle bodies along the MMT is due to partial melting of the subducting India plate triggered by the slab break-off (Hussain et al., 2018). Thus, the studied syenite and pegmatite were likely to form from partial melting of metasomatized lithospheric mantle induced by the asthenospheric upwelling due to the slab break-off during the post-collisional stage (Fig. 13b).

The Tethyan orogenic belt contains the whole record of magmatism linked to the subduction of Tethyan oceanic crust, followed by continental collision, crustal subduction, and accretion. Post-collisional alkaline rocks are widely distributed in many places along the Tethyan orogenic belt (e.g., Ersoy and Palmer, 2013; Zhu et al., 2018). Those post-collisional alkaline rocks in the Tethyan orogeny should be good targets for REE exploration.

7. Conclusion

461 (1) The syenite and pegmatite from the Kohistan Batholith in the Kohistan Island Arc
462 in Pakistan host economically exploitable REE mineralization. U-Th-Pb dating
463 indicates that the syenite and the pegmatite were emplaced at ca. 30–31 Ma. Similarity
464 in zircon Hf isotopic compositions demonstrates that the syenite and the pegmatite are
465 coeval and co-magmatic in origin.
466 (2) The main REE minerals (chevkinite and monazite) in the pegmatite are magmatic
467 genesis. Zircon trace elemental geochemistry reveals that magma evolution from the
468 syenite to the pegmatite was marked by increasing Hf, Ce*, Ce^{4+}/Ce^{3+}, Yb, Y and U
469 contents, but decreasing Ti and Eu* contents.
470 (3) The alkaline magma in the KIA was derived from an enriched lithospheric mantle
471 due to the slab break-off during the post-collisional stage. The lithospheric mantle in
472 the KIA might have been metasomatised during the preceding subduction event. Post-
473 collisional alkaline rocks in the Tethyan orogeny are good targets for REE exploration.
474

475 **Declaration of Competing Interest**

476 The authors declare that they have no known competing financial interests or personal
477 relationships that could have appeared to influence the work reported in this paper.
478

479 **Acknowledgments**

480 This study is supported by the National Natural Science Foundation of China Project
481 (No. 91755208, 41673043), the National Key R & D Plan (No. 2017YFC0601404) and
482 the special fund from the State Key Laboratory of Geological Processes and Mineral

Resources (No. MSFGPMR03-2). The authors would like to express their sincere gratitude to Editor-in-chief Prof. Franco Pirajno, Associate Editor Dr. Alla Dolgopolova and two anonymous reviewers for their helpful comments and suggestions.

References

Ballard, J. R., Palin, M. J., Campbell, I. H., 2002. Relative oxidation states of magmas inferred from Ce(IV)/Ce(III) in zircon: application to porphyry copper deposits of northern Chile. Contributions to Mineralogy and Petrology 144 (3), 347–364.

Belousova, E., Griffin, W., O'Reilly, S. Y., 2005. Zircon crystal morphology, trace element signatures and Hf isotope composition as a tool for petrogenetic modelling: examples from Eastern Australian granitoids. Journal of Petrology 47 (2), 329–353.

Bouvier, A., Vervoort, J. D., Patchett, P. J., 2008. The Lu-Hf and Sm-Nd isotopic composition of CHUR: constraints from unequilibrated chondrites and implications for the bulk composition of terrestrial planets. Earth and Planetary Science Letters 273 (1-2), 48–57.

Breiter, K., Förster, H.-J., Škoda, R., 2006. Extreme P-, Bi-, Nb-, Sc-, U-and F-rich zircon from fractionated perphosphorous granites: The peraluminous Podlesí granite system, Czech Republic. Lithos 88 (1-4), 15–34.

Burg, J.-P., Arbaret, L., Chaudhry, N., Dawood, H., Hussain, S., Zeilinger, G., 2005. Shear strain localization from the upper mantle to the middle crust of the

505 Kohistan Arc (Pakistan). Geological Society of London, Special Publications
506 245 (1), 25–38.
507 Burg, J.-P., 2011. The Asia-Kohistan-India collision: Review and Discussion. In:
508 Brown, D. and Ryan, P.D. (eds.), Arc-Continent Collision. Frontiers in Earth
509 Sciences, Springer-Verlag Berlin Heidelberg, Chapter 10, 279-309.
510 Černý, P., Ercit, T. S., 2005. The classification of granitic pegmatites revisited. The
511 Canadian Mineralogist 43 (6), 2005–2026.
512 Černý, P., Meintzer, R. E., Anderson, A. J., 1985. Extreme fractionation in rare-element
513 granitic pegmatites; selected examples of data and mechanisms. The Canadian
514 Mineralogist 23 (3), 381–421.
515 Černý, P., Teertstra, D., Chapman, R., Selway, J., Hawthorne, F., Ferreira, K.,
516 Chackowsky, L., Wang, X., Meintzer, R., Mineralogist, C., 2012. Extreme
517 fractionation and deformation of the leucogranite-pegmatite suite at Red Cross
518 Lake, Manitoba, Canada. Canadian Mineralogist 50 (6), 9187–9192.
519 Chakhmouradian, A. R., Zaitsev, A. N., 2012. Rare earth mineralization in igneous
520 rocks: sources and processes. Elements 8 (5), 347–353.
521 Chu, N.-C., Taylor, R. N., Chavagnac, V., Nesbitt, R. W., Boella, R. M., Milton, J. A.,
522 German, C. R., Bayon, G., Burton, K., 2002. Hf isotope ratio analysis using
523 multi-collector inductively coupled plasma mass spectrometry: an evaluation of
524 isobaric interference corrections. Journal of Analytical Atomic Spectrometry 17
525 (12), 1567–1574.

526 Claiborne, L. L., Miller, C. F., Wooden, J. L., 2010. Trace element composition of
527 igneous zircon: a thermal and compositional record of the accumulation and
528 evolution of a large silicic batholith, Spirit Mountain, Nevada. Contributions to
529 Mineralogy and Petrology 160 (4), 511–531.
530 Clemens, J., Holloway, J. R., White, A., 1986. Origin of an A-type granite;
531 experimental constraints. American Mineralogist 71 (3-4), 317–324.
532 Coward, M. P., Rex, D. C., Khan, M. A., Windley, B. F., Broughton, R. D., Luff, I. W.,
533 Petterson, M. G., Pudsey, C. J., 1986. Collision tectonics in the NW Himalayas.
534 Geological Society of London, Special Publications 19 (1), 203–219.
535 Dostal, J., 2016. Rare metal deposits associated with alkaline/peralkaline igneous rocks.
536 Reviews in Economic Geology 18, 33–54.
537 Dostal, J., 2017. Rare earth element deposits of alkaline igneous rocks. Resources 6 (3),
538 34.
539 Dostal, J., Kontak, D. J., Karl, S. M., 2014. The Early Jurassic Bokan Mountain
540 peralkaline granitic complex (southeastern Alaska): Geochemistry,
541 petrogenesis and rare-metal mineralization. Lithos 202, 395–412.
542 Ersoy, E.Y., Palmer, M.R., 2013. Eocene-Quaternary magmatic activity in the Aegean:
543 Implications for mantle metasomatism and magma genesis in an evolving
544 orogeny. Lithos 180-181, 5-24.
545 Ferry, J., Watson, E., 2007. New thermodynamic models and revised calibrations for
546 the Ti-in-zircon and Zr-in-rutile thermometers. Contributions to Mineralogy
547 and Petrology 154 (4), 429–437.

548 Günther, D., Hattendorf, B., 2005. Solid sample analysis using laser ablation
549 inductively coupled plasma mass spectrometry. Trends in Analytical Chemistry
550 24 (3), 255–265.
551 Harlov, D. E., Wirth, R., Hetherington, C. J., 2011. Fluid-mediated partial alteration in
552 monazite: the role of coupled dissolution-reprecipitation in element
553 redistribution and mass transfer. Contributions to Mineralogy and Petrology 162
554 (2), 329–348.
555 Hoskin, P. W., 2005. Trace-element composition of hydrothermal zircon and the
556 alteration of Hadean zircon from the Jack Hills, Australia. Geochimica et
557 Cosmochimica Acta 69 (3), 637–648.
558 Hoskin, P. W., Kinny, P. D., Wyborn, D., Chappell, B. W., 2000. Identifying accessory
559 mineral saturation during differentiation in granitoid magmas: an integrated
560 approach Journal of Petrology. 41 (9), 1365–1396.
561 Hoskin, P. W., Schaltegger, U., 2003. The composition of zircon and igneous and
562 metamorphic petrogenesis. Reviews in Mineralogy and Geochemistry 53 (1),
563 27–62.
564 Hou, Z.Q., Liu, Y., Tian, S.H., Yang, Z.M., Xie, Y.L., 2015. Formation of carbonatite-
565 related giant rare-earth-element deposits by the recycling of marine sediments.
566 Scientific Reports 5, 10231.
567 Hu, Z., Gao, S., Liu, Y., Hu, S., Chen, H., Yuan, H., 2008. Signal enhancement in laser
568 ablation ICP-MS by addition of nitrogen in the central channel gas. Journal of
569 Analytical Atomic Spectrometry 23 (8), 1093–1101.

570 Hussain, S.S.T., Zhao, J.M., Xiao, Q.B., Imran, B.Z., Khan, N.G., Zhang, H., Deng,
571 G., Liu, H.B., 2018. Electrical resistivity structures and tectonic implications
572 of Main Karakorum Thrust (MKT) in the western Himalayas: NNE Pakistan.
573 Phy. Earth Planet. Inter. 279, 57–66.
574 Jagoutz, O., Bouilhol, P., Schaltegger, U., Müntener, O., 2018. The isotopic evolution
575 of the Kohistan Ladakh arc from subduction initiation to continent arc collision.
576 Geological Society of London, Special Publications 483, 487.
577 Jagoutz, O., Müntener, O., Ulmer, P., Pettke, T., Burg, J.-P., Dawood, H., Hussain, S.,
578 2007. Petrology and mineral chemistry of lower crustal intrusions: the Chilas
579 Complex, Kohistan (NW Pakistan). Journal of Petrology 48 (10), 1895–1953.
580 Kempe, U., Götze, J., Dandar, S., Habermann, D., 1999. Magmatic and metasomatic
581 processes during formation of the Nb-Zr-REE deposits Khaldzan Buregte and
582 Tsakhir (Mongolian Altai): Indications from a combined CL-SEM study.
583 Mineralogical Magazine 63 (2), 165–177.
584 Khan, M. A., 1989. The Chilas mafic-ultramafic igneous complex: The root of the
585 Kohistan Island Arc in the Himalaya of northern Pakistan. Geological Society
586 of America, Special papers 232, 75.
587 Lee, R. G., Dilles, J. H., Tosdal, R. M., Wooden, J. L., Mazdab, F. K., 2017. Magmatic
588 evolution of granodiorite intrusions at the El Salvador porphyry copper deposit,
589 Chile, based on trace element composition and U/Pb age of zircons. Economic
590 Geology 112 (2), 245–273.

591 Li, W., Cheng, Y., Yang, Z., 2019. Geo−fO_2: Integrated software for analysis of
592 magmatic oxygen fugacity. Geochemistry, Geophysics, Geosystems 20, 2542–
593 2555.
594 Li, X. H., Long, W. G., Li, Q. L., Liu, Y., Zheng, Y. F., Yang, Y. H., Chamberlain, K.
595 R., Wan, D. F., Guo, C. H., Wang, X. C., 2010. Penglai zircon megacrysts: a
596 potential new working reference material for microbeam determination of Hf-
597 O isotopes and U-Pb age. Geostandards and Geoanalytical Research 34 (2),
598 117–134.
599 Linnen, R. L., Keppler, H., 1997. Columbite solubility in granitic melts: consequences
600 for the enrichment and fractionation of Nb and Ta in the Earth's crust.
601 Contributions to Mineralogy and Petrology 128 (2-3), 213–227.
602 Liu, Y., Gao, S., Hu, Z., Gao, C., Zong, K., Wang, D., 2010. Continental and oceanic
603 crust recycling-induced melt-peridotite interactions in the Trans-North China
604 Orogen: U-Pb dating, Hf isotopes and trace elements in zircons from mantle
605 xenoliths. Journal of Petrology 51 (1-2), 537–571.
606 Liu, Y., Hu, Z., Gao, S., Günther, D., Xu, J., Gao, C., Chen, H., 2008. In situ analysis
607 of major and trace elements of anhydrous minerals by LA-ICP-MS without
608 applying an internal standard. Chemical Geology 257 (1-2), 34–43.
609 Liziero, F., 2008. Studio Cristallochimico E Strutturale Di Chevkiniti-(Ce) Non
610 Metamittiche. Ph.D. Thesis, University of Padua.
611 London, D., 2018. Ore-forming processes within granitic pegmatites. Ore Geol. Rev.
612 101, 349–383.

613 Ludwig, K. R., 2003. A geochronlogical toolkit for microsoft excel. Special
614 Publication Berkeley Geochrology Center 1, 1–70.
615 Macdonald, R., Bagiński, B., Dzierżanowski, P., Fettes, D. J., Upton, B. G., 2013.
616 Chevkinite-group minerals in UK Palaeogene granites: underestimated REE-
617 bearing accessory phases. The Canadian Mineralogist 51 (2), 333–347.
618 MacDonald, R., Belkin, H., 2002. Compositional variation in minerals of the chevkinite
619 group. Mineralogical Magazine 66 (6), 1075–1098.
620 Marks, M. A., Markl, G., 2017. A global review on agpaitic rocks. Earth-Science
621 Reviews 173, 229–258.
622 Molnar, P., Tapponnier, P., 1975. Cenozoic tectonics of Asia: effects of a continental
623 collision. Science 189 (4201), 419–426.
624 Petterson, M. G., 2010. A review of the geology and tectonics of the Kohistan island
625 arc, north Pakistan. Geological Society, London, Special Publications 338 (1),
626 287–327.
627 Petterson, M. G., Windley, B. F., 1985. Rb-Sr dating of the Kohistan arc-batholith in
628 the Trans-Himalaya of north Pakistan, and tectonic implications. Earth and
629 Planetary Science Letters 74 (1), 45–57.
630 Rehman, H. U., Seno, T., Yamamoto, H., Khan, T., 2011. Timing of collision of the
631 Kohistan–Ladakh Arc with India and Asia: debate. Island Arc 20 (3), 308–328.
632 Siegel, K., Vasyukova, O. V., Williams-Jones, A. E., 2018. Magmatic evolution and
633 controls on rare metal-enrichment of the Strange Lake A-type peralkaline
634 granitic pluton, Québec-Labrador. Lithos 308, 34–52.

635 Söderlund, U., Patchett, P. J., Vervoort, J. D., Isachsen, C. E., 2004. The ^{176}Lu decay
636 constant determined by Lu-Hf and U-Pb isotope systematics of Precambrian
637 mafic intrusions. Earth and Planetary Science Letters 219 (3-4), 311–324.
638 Stepanov, A., Mavrogenes, J. A., Meffre, S., Davidson, P., 2014. The key role of mica
639 during igneous concentration of tantalum. Contributions to Mineralogy and
640 Petrology 167 (6), 1–8.
641 Thomas, J., Bodnar, R., Shimizu, N., Sinha, A., 2002. Determination of zircon/melt
642 trace element partition coefficients from SIMS analysis of melt inclusions in
643 zircon. Geochimica et Cosmochimica Acta 66 (16), 2887–2901.
644 Tillberg, M., Maskenskaya, O. M., Drake, H., Hogmalm, J. K., Broman, C., Fallick, A.
645 E., Åström, M. E., 2019. Fractionation of rare earth elements in greisen and
646 hydrothermal veins related to A-type magmatism. Geofluids 2019, 1–20.
647 Tomascak, P. B., Krogstad, E. J., Walker, R. J., 1996. U-Pb monazite geochronology
648 of granitic rocks from Maine: implications for late Paleozoic tectonics in the
649 Northern Appalachians. The Journal of Geology 104 (2), 185–195.
650 Trail, D., Watson, E. B., Tailby, N. D., 2012. Ce and Eu anomalies in zircon as proxies
651 for the oxidation state of magmas. Geochimica et Cosmochimica Acta 97, 70–
652 87.
653 Treloar, P., Broughton, R., Williams, M., Coward, M., Windley, B., 1989. Deformation,
654 metamorphism and imbrication of the Indian plate, south of the Main Mantle
655 Thrust, north Pakistan. Journal of Metamorphic Geology 7 (1), 111–125.

Treloar, P. J., Petterson, M. G., Jan, M. Q., Sullivan, M., 1996. A re-evaluation of the stratigraphy and evolution of the Kohistan arc sequence, Pakistan Himalaya: implications for magmatic and tectonic arc-building processes. Journal of the Geological Society of London 153 (5), 681–693.

Uher, P., Černý, P., 1998. Zircon in Hercynian granitic pegmatites of the Western Carpathians, Slovakia. Geologica Carpathica 49, 261–270.

Veksler, I. V., Dorfman, A. M., Kamenetsky, M., Dulski, P., Dingwell, D. B., 2005. Partitioning of lanthanides and Y between immiscible silicate and fluoride melts, fluorite and cryolite and the origin of the lanthanide tetrad effect in igneous rocks. Geochimica et Cosmochimica Acta 69 (11), 2847–2860.

Wark, D. A., Miller, C. F., 1993. Accessory mineral behavior during differentiation of a granite suite: monazite, xenotime and zircon in the Sweetwater Wash pluton, southeastern California, USA. Chemical Geology 110 (1-3), 49–67.

Watson, E., Wark, D., Thomas, J., 2006. Crystallization thermometers for zircon and rutile. Contributions to Mineralogy and Petrology 151 (4), 413–433.

Watson, E. B., Harrison, T., 2005. Zircon thermometer reveals minimum melting conditions on earliest Earth. Science 308 (5723), 841–844.

Wiedenbeck, M., Alle, P., Corfu, F., Griffin, W., Meier, M., Oberli, F., Quadt, A. v., Roddick, J., Spiegel, W., 1995. Three natural zircon standards for U-Th-Pb, Lu-Hf, trace element and REE analyses. Geostandards Newsletter 19 (1), 1–23.

676 Williams-Jones, A. E., Migdisov, A. A., Samson, I. M., 2012. Hydrothermal
677 mobilisation of the rare earth elements-a tale of “ceria” and “yttria”. Elements
678 8 (5), 355–360.
679 Ying, Y.C., Chen, W., Simonetti, A., Jiang, S.Y., Zhao, K.D., 2020. Significance of
680 hydrothermal reworking for REE mineralization associated with carbonatite:
681 Constraints from in situ trace element and C-Sr isotope study of calcite and
682 apatite from the Miaoya carbonatite complex (China). Geochim. Cosmochim.
683 Acta 280, 340–359.
684 Zhu, D.C., Wang, Q., Chung, S.L., Cawood, P.A., Zhao, Z.D., 2018. Gangdese
685 magmatism in southern Tibet and India-Asia convergenece since 120 Ma.
686 Treloar, P.J. and Searle, M.P. (eds.), Himalayan Tectonics: A modern Synthesis.
687 Geological Society, London, Special Publications 483.

688 **Table 1 LA-ICP-MS U-Th-Pb isotopic dating results of zircons from the syenite and the pegmatite**

689

Spots	Th (ppm)	U (ppm)	Th/U	$^{238}U/^{232}Th$	$^{207}Pb/^{206}Pb$		$^{207}Pb/^{235}U$		$^{206}Pb/^{238}U$		$^{207}Pb/^{206}Pb$		$^{207}Pb/^{235}U$		$^{206}Pb/^{238}U$		
					Ratio	1sigma	Ratio	1sigma	Ratio	1sigma	Age (Ma)	1sigma	Age (Ma)	1sigma	Age (Ma)	1sigma	Concordance
Zircons from the syenite																	
T37-1	1984.4	2649.6	0.75	1.382	0.0498	0.0034	0.0325	0.0020	0.00473	0.00007	183.4	163.9	32.4	2.0	30.4	0.5	93%
T37-3	1516.6	2078.1	0.73	1.406	0.0432	0.0029	0.0280	0.0017	0.00474	0.00008	590.3	182.4	28.0	1.7	30.5	0.5	91%
T37-8	37.4	425.2	0.09	12.054	0.0671	0.0083	0.0417	0.0038	0.00496	0.00016	838.9	258.2	41.5	3.7	31.9	1.0	73%
T37-9	967.7	1812.6	0.53	1.925	0.0504	0.0044	0.0334	0.0029	0.00479	0.00008	213.0	192.6	33.3	2.8	30.8	0.5	92%
T37-10	3041.0	3601.1	0.84	1.222	0.0505	0.0022	0.0355	0.0016	0.00508	0.00007	220.4	99.1	35.4	1.6	31.7	0.4	92%
T37-11	1288.3	1094.0	1.18	0.873	0.0498	0.0042	0.0325	0.0021	0.00480	0.00010	187.1	185.2	32.4	2.1	30.8	0.6	94%
T37-14	845.4	1562.2	0.54	1.946	0.0533	0.0039	0.0346	0.0022	0.00478	0.00009	338.9	164.8	34.6	2.1	30.7	0.6	88%
T37-15	1030.1	1420.2	0.73	1.452	0.0712	0.0140	0.0436	0.0056	0.00485	0.00011	964.8	411.9	43.4	5.4	31.2	0.7	67%
T37-17	1762.5	2518.0	0.70	1.485	0.0505	0.0032	0.0326	0.0021	0.00472	0.00009	216.7	152.8	32.6	2.1	30.4	0.6	92%
T37-18	944.3	1086.2	0.87	1.203	0.0531	0.0048	0.0338	0.0027	0.00483	0.00011	344.5	202.8	33.8	2.6	31.0	0.7	91%
T37-19	225.7	1647.6	0.14	7.496	0.0569	0.0037	0.0367	0.0022	0.00480	0.00008	487.1	141.6	36.6	2.1	30.9	0.5	82%
T37-20	372.6	513.8	0.73	1.404	0.0610	0.0121	0.0340	0.0040	0.00523	0.00016	638.9	437.0	34.0	4.0	31.6	1.0	98%
T37-21	532.9	800.7	0.67	1.538	0.0431	0.0043	0.0278	0.0020	0.00487	0.00012	286.0	150.6	27.8	2.0	31.3	0.8	88%
T37-22	1421.9	3073.0	0.46	2.247	0.0474	0.0031	0.0319	0.0018	0.00491	0.00007	77.87	135.2	31.9	1.8	31.6	0.4	98%
T37-24	407.1	746.9	0.55	1.872	0.0426	0.0050	0.0287	0.0026	0.00491	0.00013	224.4	99.1	28.7	2.6	31.6	0.8	90%
T25-13	953.4	1207.8	0.79	1.999	0.0577	0.0035	0.0385	0.0023	0.00488	0.00009	520.4	133.3	38.3	2.3	31.4	0.6	79%
T25-18	674.9	1166.9	0.58	2.040	0.0631	0.0042	0.0430	0.0028	0.00496	0.00009	722.2	144.4	42.7	2.7	31.9	0.6	71%
T25-13	953.4	1207.8	0.79	1.999	0.0577	0.0035	0.0385	0.0023	0.00488	0.00009	520.4	133.3	38.3	2.3	31.4	0.6	79%
T29-22	155.4	1290.7	0.12	9.093	0.0545	0.0027	0.0370	0.0018	0.00497	0.00011	390.8	111.1	36.9	1.8	32.0	0.7	85%
T29-14	690.3	1550.8	0.45	2.418	0.0531	0.0029	0.0358	0.0020	0.00490	0.00006	344.5	124.1	35.7	2.0	31.5	0.4	87%

Zircons from the pegmatite

T16-1	**1220.0**	**7944.9**	**0.15**	**7.071**	**0.049**	**0.001**	**0.0321**	**0.0010**	**0.00473**	**0.00005**	**200.1**	**66.7**	**32.1**	**1.0**	**30.4**	**0.4**	**94%**
T16-2	**124.3**	**1777.9**	**0.07**	**15.898**	**0.053**	**0.003**	**0.0351**	**0.0019**	**0.00483**	**0.00009**	**324.1**	**111.1**	**35.0**	**1.8**	**31.0**	**0.5**	**88%**
T16-4	**1193.5**	**7198.4**	**0.17**	**6.421**	**0.047**	**0.002**	**0.0296**	**0.0010**	**0.00456**	**0.00006**	**57.50**	**142.6**	**29.6**	**0.9**	**30.0**	**0.4**	**99%**
T16-5	**111.4**	**2820.8**	**0.04**	**26.740**	**0.057**	**0.003**	**0.0369**	**0.0016**	**0.00470**	**0.00007**	**483.4**	**93.5**	**36.8**	**1.6**	**30.2**	**0.4**	**80%**
T16-6	**1614.3**	**10716.9**	**0.15**	**7.154**	**0.047**	**0.001**	**0.0303**	**0.0009**	**0.00460**	**0.00005**	**77.87**	**100.0**	**30.3**	**0.8**	**30.0**	**0.3**	**97%**
T16-8	**2210.6**	**8221.1**	**0.27**	**4.155**	**0.045**	**0.001**	**0.0289**	**0.0009**	**0.00459**	**0.00005**	**77.77**	**28.9**	**28.9**	**0.9**	**29.5**	**0.3**	**98%**
T37-1	**780.7**	**3056.0**	**0.26**	**1.448**	**0.057**	**0.003**	**0.0364**	**0.0020**	**0.00469**	**0.00008**	**501.9**	**129.6**	**36.3**	**2.0**	**30.2**	**0.5**	**81%**
T37-2	**572.5**	**1123.2**	**0.51**	**2.099**	**0.057**	**0.004**	**0.0380**	**0.0023**	**0.00485**	**0.00010**	**501.9**	**132.4**	**37.9**	**2.3**	**30.2**	**0.6**	**80%**
T11-5	**254.8**	**910.2**	**0.28**	**4.934**	**0.055**	**0.005**	**0.0352**	**0.0030**	**0.00464**	**0.00009**	**433.4**	**182.4**	**35.2**	**2.9**	**29.9**	**0.6**	**83%**
T3-4	**696.5**	**1189.7**	**0.59**	**1.837**	**0.054**	**0.004**	**0.0352**	**0.0023**	**0.00475**	**0.00009**	**390.8**	**144.4**	**35.1**	**2.2**	**30.5**	**0.6**	**86%**

690

691

692 **Table 2 LA-ICP-MS U-Th-Pb isotopic dating results of monazites from the pegmatite**

693

Spots	Pb	Th	U	Th/U	$^{207}Pb/^{235}U$		$^{206}Pb/^{238}U$		$^{208}Pb/^{232}Th$		$^{207}Pb/^{235}U$		$^{206}Pb/^{238}U$		$^{208}Pb/^{232}Th$	
	(ppm)	(ppm)	(ppm)		Ratio	2sigma	Ratio	2sigma	Ratio	2sigma	Age (Ma)	2sigma	Age (Ma)	2sigma	Age (Ma)	2sigma
T1-1	12.3	9373	92.9	100.9	0.1389	0.0350	0.0054	0.0006	0.00148	0.00004	132.1	31.2	34.4	4.1	29.9	0.8
T1-2	9.3	6634	59.0	112.4	0.2431	0.0634	0.0072	0.0011	0.00156	0.00004	220.9	51.7	46.1	6.9	31.6	0.9
T1-3	8.3	6007	48.4	124.1	0.2877	0.0611	0.0077	0.0011	0.00154	0.00005	256.7	48.2	49.3	7.1	31.1	1.0
T1-4	7.4	5366	41.8	128.3	0.4174	0.0910	0.0079	0.0010	0.00153	0.00004	354.2	65.2	50.6	6.3	30.9	0.9
T1-5	6.8	4874	39.8	122.5	0.2997	0.0592	0.0073	0.0008	0.00156	0.00005	266.2	46.2	47.1	5.1	31.5	1.0
T1-6	5.62	3882	32.6	119.2	0.5341	0.0994	0.0090	0.0012	0.00158	0.00006	434.5	65.8	57.7	7.8	32.0	1.2
T3-2	7.4	5371	33.7	159.2	0.4589	0.0911	0.0074	0.0009	0.00154	0.00005	383.5	63.4	47.4	5.9	31.2	0.9
T3-4	10.0	7724	59.0	130.9	0.3064	0.0479	0.0067	0.0007	0.00146	0.00004	271.4	37.2	43.3	4.5	29.5	0.8
T9-1	10.8	8033	76.3	105.3	0.1508	0.0272	0.0055	0.0006	0.00153	0.00005	142.6	24.0	35.2	3.6	30.8	0.9
T9-2	10.3	7506	69.6	107.9	0.2373	0.0563	0.0068	0.0008	0.00155	0.00004	216.2	46.2	43.7	5.1	31.2	0.8
T9-3	9.9	7512	67.9	110.6	0.2500	0.0632	0.0062	0.0007	0.00147	0.00004	226.6	51.3	40.0	4.7	29.7	0.7
T9-4	8.9	6936	61.3	113.1	0.1324	0.0334	0.0055	0.0007	0.00146	0.00004	126.2	30.0	35.6	4.4	29.4	0.8
T9-5	5.6	3913	35.8	109.4	0.3801	0.0700	0.0074	0.0010	0.00159	0.00005	327.1	51.5	47.4	6.1	32.2	1.0
T9-6	10.4	7863	72.3	108.8	0.1469	0.0289	0.0062	0.0007	0.00150	0.00004	139.2	25.6	39.7	4.3	30.3	0.8
T9-7	5.39	3755	35.6	105.6	0.4080	0.0778	0.0086	0.0010	0.00159	0.00005	347.4	56.1	55.3	6.7	32.0	1.1
T9-8	7.8	5742	47.7	120.3	0.2609	0.0600	0.0066	0.0007	0.00153	0.00004	235.4	48.3	42.7	4.8	30.9	0.8
T11-2	6.0	4333	46.4	93.4	0.2657	0.0555	0.0074	0.0009	0.00153	0.00005	239.3	44.5	47.4	5.5	30.9	1.0
T11-4	10.3	7672	69.0	111.2	0.1889	0.0468	0.0060	0.0007	0.00152	0.00004	175.7	40.0	38.4	4.7	30.7	0.8
T11-5	10.1	7379	70.2	105.1	0.2072	0.0335	0.0067	0.0007	0.00154	0.00004	191.2	28.1	42.8	4.5	31.2	0.9
T11-6	8.9	6423	59.7	107.6	0.2262	0.0516	0.0062	0.0007	0.00157	0.00005	207.0	42.8	39.9	4.6	31.8	1.0
T11b-7	6.5	4670	50.1	93.2	0.2473	0.0470	0.0068	0.0008	0.00155	0.00005	224.3	38.3	43.9	5.1	31.4	0.9
T11b-8	9.8	7182	68.5	104.8	0.2083	0.0369	0.0059	0.0006	0.00154	0.00004	192.1	31.0	37.7	3.8	31.2	0.8
T11-9	8.6	6137	54.7	112.3	0.3138	0.0595	0.0066	0.0008	0.00157	0.00005	277.1	46.0	42.4	5.3	31.7	0.9
T11-10	11.2	8156	80.0	102.0	0.1575	0.0349	0.0060	0.0007	0.00156	0.00004	148.5	30.7	38.7	4.6	31.4	0.9

T16-1	**10.3**	**7535**	**76.6**	**98.4**	**0.1390**	**0.0349**	**0.0065**	**0.0006**	**0.00155**	**0.00004**	**132.1**	**31.1**	**41.5**	**3.9**	**31.3**	**0.7**
T16-2	**6.8**	**5127**	**45.5**	**112.6**	**0.2529**	**0.0607**	**0.0066**	**0.0008**	**0.00151**	**0.00004**	**228.9**	**49.2**	**42.5**	**5.4**	**30.5**	**0.9**
T16-3	**6.9**	**5120**	**42.4**	**120.7**	**0.2060**	**0.0508**	**0.0061**	**0.0009**	**0.00156**	**0.00005**	**190.2**	**42.7**	**39.1**	**5.5**	**31.4**	**1.0**

694

695

696 **Table 3 Zircon trace element compositions of the syenite and pegmatite**

697

	Zircons from the syenite														
Spots	**T29-11**	**T29-13**	**T29-14**	**T-29-15**	**T29-17**	**T29-18**	**T29-19**	**T37-3**	**T37-4**	**T37-10**	**T37-11**	**T37-13**	**T37-16**	**T37-17**	**T37-22**
Ti	**1.89**	**1.42**	**2.78**	**1.82**	**2.06**	**1.42**	**2.01**	**2.51**	**1.74**	**2.04**	**0.88**	**1.94**	**1.71**	**3.58**	**1.68**
Y	**464.6**	**420.4**	**777.5**	**438.0**	**816.6**	**1124**	**202.9**	**785.5**	**193.7**	**2450**	**1245**	**822.1**	**495.2**	**697.1**	**1050**
La	**0.01**	**0.03**	**0.06**	**0.02**	**0.02**	**0.07**	**0.06**	**0.06**	**0.03**	**0.12**	**0.08**	**0.08**	**0.03**	**0.09**	**0.01**
Ce	**90.70**	**81.09**	**135.0**	**100.8**	**178.4**	**110.5**	**17.77**	**229.0**	**17.27**	**448.8**	**152.9**	**273.0**	**121.6**	**203.9**	**167.6**
Pr	**0.62**	**0.72**	**0.98**	**0.41**	**0.83**	**1.17**	**0.10**	**1.72**	**0.12**	**3.72**	**1.63**	**2.46**	**0.56**	**1.86**	**1.46**
Nd	**5.54**	**4.94**	**12.82**	**6.25**	**12.29**	**15.92**	**1.47**	**15.65**	**1.48**	**46.31**	**18.44**	**22.38**	**5.89**	**17.24**	**9.93**
Sm	**6.72**	**6.71**	**14.79**	**7.23**	**15.27**	**20.23**	**0.74**	**15.88**	**2.05**	**54.65**	**22.44**	**20.32**	**6.83**	**16.61**	**14.50**
Eu	**3.03**	**3.06**	**6.79**	**3.44**	**6.82**	**8.85**	**0.48**	**8.61**	**1.29**	**30.27**	**12.26**	**9.75**	**3.90**	**7.19**	**7.85**
Gd	**17.64**	**17.54**	**37.41**	**18.95**	**38.68**	**50.19**	**4.33**	**45.68**	**8.52**	**155.52**	**66.87**	**53.28**	**21.85**	**45.37**	**47.74**
Tb	**4.47**	**4.13**	**8.58**	**4.41**	**8.58**	**11.39**	**1.53**	**9.53**	**1.89**	**31.20**	**14.20**	**10.28**	**4.89**	**9.23**	**11.07**
Dy	**42.66**	**39.44**	**81.41**	**42.56**	**79.89**	**109.1**	**18.95**	**82.86**	**17.86**	**262.4**	**121.1**	**83.90**	**44.50**	**74.60**	**99.30**
Ho	**13.42**	**12.06**	**24.15**	**12.82**	**23.97**	**32.50**	**6.99**	**24.27**	**5.80**	**76.40**	**36.63**	**24.15**	**14.61**	**22.08**	**31.68**
Er	**53.74**	**48.43**	**91.90**	**49.33**	**92.11**	**126.3**	**32.10**	**88.95**	**22.42**	**276.7**	**137.9**	**84.03**	**57.74**	**79.99**	**121.6**
Tm	**12.34**	**11.39**	**20.25**	**11.21**	**21.01**	**29.01**	**8.42**	**18.24**	**4.69**	**56.67**	**29.83**	**17.53**	**12.85**	**17.01**	**27.10**
Yb	**117.5**	**107.9**	**177.2**	**106.6**	**192.8**	**272.7**	**85.31**	**161.2**	**43.70**	**488.2**	**272.2**	**151.0**	**120.1**	**150.5**	**252.3**
Lu	**19.53**	**18.44**	**27.48**	**17.73**	**31.06**	**43.81**	**14.19**	**25.18**	**6.76**	**73.29**	**44.17**	**24.06**	**19.58**	**23.58**	**41.35**
Hf	**9879**	**9233**	**8708**	**8808**	**8639**	**8452**	**7562**	**8338**	**8533**	**8374**	**8099**	**7377**	**9365**	**7131**	**8933**
Nb	**0.91**	**0.79**	**1.00**	**0.78**	**1.35**	**0.53**	**1.54**	**1.82**	**0.63**	**1.93**	**0.98**	**2.76**	**1.28**	**2.99**	**2.96**
Ta	**0.14**	**0.13**	**0.12**	**0.12**	**0.15**	**0.11**	**0.54**	**0.15**	**0.05**	**0.12**	**0.09**	**0.13**	**0.11**	**0.16**	**0.27**
Pb	**7.03**	**5.16**	**10.72**	**6.68**	**15.72**	**10.61**	**2.33**	**20.00**	**4.11**	**39.75**	**14.85**	**20.94**	**12.12**	**33.03**	**26.76**
Th	**518.3**	**387.0**	**690.3**	**540.4**	**1295**	**862.2**	**270.3**	**1650**	**193.1**	**3322**	**1396**	**1578**	**894.4**	**2551**	**1865**
U	**666.3**	**481.1**	**1551**	**609.5**	**1515**	**828.7**	**648.3**	**2146**	**605.7**	**1797**	**1128**	**1948**	**1040**	**2925**	**3548**
Th/U	**0.78**	**0.80**	**0.45**	**0.89**	**0.85**	**1.04**	**0.04**	**0.77**	**0.32**	**0.87**	**1.24**	**0.81**	**0.86**	**0.87**	**0.53**

Hf/Y	**0.18**	**0.16**	**0.28**	**0.14**	**0.18**	**0.11**	**12.83**	**0.20**	**0.16**	**0.14**	**0.07**	**0.16**	**0.13**	**0.18**	**0.51**
LREE	**106.6**	**96.5**	**170.5**	**118.1**	**213.7**	**156.7**	**19.61**	**270.9**	**22.24**	**583.9**	**207.8**	**327.9**	**138.8**	**246.8**	**201.3**
HREE	**281.3**	**259.4**	**468.3**	**263.6**	**488.1**	**675.0**	**171.8**	**455.9**	**111.6**	**1420**	**722.9**	**448.3**	**296.2**	**422.4**	**632.1**
$(Sm/La)_N$	**786.2**	**371.6**	**414.1**	**559.0**	**1232**	**470.9**	**19.42**	**399.3**	**124.4**	**715.0**	**426.1**	**396.0**	**431.0**	**303.5**	**2509**
Ce*/Ce	**45.33**	**34.61**	**41.71**	**74.58**	**66.04**	**28.66**	**44.63**	**40.69**	**40.37**	**36.94**	**28.50**	**34.03**	**66.45**	**33.44**	**35.58**
Eu*/Eu	**0.81**	**0.82**	**0.84**	**0.85**	**0.82**	**0.81**	**0.63**	**0.91**	**0.81**	**0.94**	**0.90**	**0.86**	**0.89**	**0.75**	**0.83**
Ce^{4+}/Ce^{3+}	**281.2**	**261.1**	**150.3**	**253.4**	**208.9**	**102.7**	**556.9**	**72.16**	**75.85**	**41.99**	**43.53**	**52.34**	**139.2**	**55.71**	**104.8**
Yb/Gd	**6.66**	**6.16**	**4.74**	**5.63**	**4.98**	**5.43**	**19.70**	**3.53**	**5.13**	**3.14**	**4.07**	**2.84**	**5.50**	**3.32**	**5.28**
T_{Ti}(ºC)	**647.5**	**626.1**	**678.2**	**644.6**	**654.3**	**626.1**	**652.4**	**669.9**	**641.4**	**653.5**	**592.5**	**649.6**	**640.2**	**699.5**	**638.8**
$\log fO_2$	**-12.3**	**-14.0**	**-12.9**	**-12.9**	**-13.0**	**-17.5**	**-9.5**	**-16.1**	**-17.6**	**-19.1**	**-22.9**	**-18.5**	**-15.4**	**-15.4**	**-16.6**

698

	Zircons from the pegmatite														
Spots	**T16b-1-1**	**T16b-1-3**	**T16b-1-4**	**T16b-1-5**	**T16b-2-1**	**T16b-2-3**	**T16b-4-1**	**T16b-4-3**	**T16b-4-4**	**T16b-4-5**	**T-16-3**	**T-16-5**	**T-16-9**	**T-16-10**	**T-16-13**
Ti	**0.46**	**1.82**	**1.76**	**0.32**	**0.46**	**1.04**	**0.18**	**0.53**	**0.90**	**0.52**	**0.65**	**0.24**	**0.22**	**0.24**	**0.47**
Y	**5626**	**895**	**3448**	**524**	**4256**	**3728**	**4365**	**588.1**	**5121**	**5275**	**2548**	**3370**	**4902**	**9684**	**2811**
La	**1.52**	**0.86**	**1.88**	**1.25**	**0.25**	**0.60**	**1.31**	**0.10**	**0.01**	**0.33**	**0.24**	**0.23**	**0.10**	**0.17**	**0.46**
Ce	**787.0**	**473.5**	**333.5**	**470.9**	**367.1**	**374.8**	**269.4**	**356.5**	**453.5**	**543.5**	**154.8**	**188.4**	**334.0**	**1234**	**186.4**
Pr	**1.69**	**0.56**	**1.57**	**0.53**	**0.35**	**1.11**	**1.19**	**0.61**	**0.65**	**0.41**	**0.70**	**0.30**	**0.22**	**0.62**	**0.63**
Nd	**6.12**	**1.91**	**6.79**	**1.66**	**2.96**	**3.86**	**5.37**	**1.29**	**5.16**	**3.83**	**3.06**	**3.07**	**2.56**	**3.18**	**4.21**
Sm	**19.17**	**4.35**	**19.61**	**1.99**	**19.13**	**16.62**	**18.18**	**1.76**	**30.66**	**23.91**	**13.51**	**16.25**	**15.69**	**21.03**	**15.34**
Eu	**13.71**	**2.77**	**11.39**	**0.99**	**12.59**	**10.76**	**11.48**	**1.15**	**19.47**	**15.68**	**7.80**	**9.51**	**9.74**	**15.04**	**8.54**
Gd	**126.4**	**22.99**	**95.58**	**7.53**	**117.2**	**96.70**	**102.1**	**11.62**	**170.1**	**139.1**	**61.95**	**79.32**	**86.74**	**153.8**	**69.27**
Tb	**47.72**	**8.25**	**32.92**	**2.64**	**39.98**	**34.06**	**36.79**	**4.55**	**53.99**	**48.64**	**21.67**	**27.60**	**34.80**	**69.41**	**24.39**
Dy	**573.8**	**94.62**	**366.2**	**35.00**	**453.4**	**388.5**	**424.4**	**56.00**	**569.4**	**548.8**	**258.8**	**336.8**	**467.3**	**975.2**	**291.3**
Ho	**203.1**	**32.59**	**127.7**	**14.57**	**155.8**	**135.4**	**155.2**	**20.98**	**190.5**	**189.7**	**91.50**	**121.6**	**175.2**	**367.4**	**102.9**
Er	**858.6**	**137.7**	**578.7**	**76.35**	**684.6**	**594.2**	**705.4**	**91.04**	**813.8**	**812.1**	**425.1**	**567.2**	**809.8**	**1554**	**472.7**
Tm	**193.1**	**33.71**	**161.8**	**21.38**	**183.0**	**158.4**	**193.5**	**23.35**	**228.8**	**211.3**	**113.6**	**147.2**	**185.4**	**292.2**	**121.0**

Yb	**1616**	**312.9**	**1948**	**229.5**	**2075**	**1786**	**2218**	**225.3**	**2894**	**2295**	**1363**	**1688**	**1750**	**2333**	**1368**
Lu	**237.9**	**49.9**	**377.6**	**40.35**	**385.4**	**320.5**	**422.9**	**35.47**	**591.8**	**412.7**	**282.7**	**335.9**	**300.3**	**369.8**	**262.0**
Hf	**10241**	**8881**	**9284**	**8440**	**9404**	**9910**	**9256**	**6823**	**8176**	**9754**	**9325**	**9081**	**9743**	**9425**	**9462**
Nb	**77.83**	**3.78**	**15.16**	**20.91**	**57.23**	**51.44**	**22.14**	**6.94**	**68.69**	**82.27**	**17.33**	**19.94**	**25.62**	**69.24**	**24.84**
Ta	**7.36**	**1.00**	**1.40**	**0.62**	**2.67**	**2.48**	**1.81**	**1.21**	**2.49**	**4.50**	**1.04**	**1.29**	**2.46**	**3.10**	**1.23**
Pb	**35.42**	**11.57**	**30.13**	**16.02**	**26.39**	**36.87**	**28.61**	**17.87**	**37.97**	**36.29**	**24.61**	**26.03**	**22.48**	**22.52**	**32.23**
Th	**2879**	**200.3**	**1228**	**125.1**	**1201**	**1447**	**1348**	**111.1**	**1621**	**2219**	**781.2**	**940.9**	**1218**	**1335**	**825.7**
U	**5458**	**2221**	**7998**	**3790**	**7244**	**7240**	**7094**	**2833**	**10763**	**8257**	**5073**	**6566**	**4796**	**3070**	**5620**
Th/U	**0.53**	**0.09**	**0.15**	**0.07**	**0.17**	**0.20**	**0.19**	**0.04**	**0.15**	**0.27**	**0.15**	**0.14**	**0.25**	**0.44**	**0.15**
Hf/Y	**1.82**	**9.92**	**2.69**	**16.09**	**2.21**	**2.66**	**2.12**	**11.60**	**1.60**	**1.85**	**3.66**	**2.69**	**1.99**	**0.97**	**3.37**
LREE	**829.2**	**483.9**	**374.7**	**477.3**	**402.3**	**407.8**	**306.9**	**361.4**	**509.4**	**587.7**	**180.1**	**217.8**	**362.3**	**1274**	**215.0**
HREE	**3856**	**692.6**	**3688**	**427.3**	**4095**	**3514**	**4258**	**468.3**	**5512**	**4657**	**2618**	**3304**	**3809**	**6114**	**2712**
$(Sm/La)_N$	**20.05**	**8.02**	**16.63**	**2.54**	**121.4**	**43.80**	**22.18**	**29.54**	**9277**	**115.5**	**89.13**	**111.9**	**247.6**	**194.2**	**53.03**
Ce*/Ce	**106.1**	**126.0**	**44.5**	**142.2**	**255.3**	**86.3**	**48.7**	**171.0**	**216.8**	**311.7**	**260.5**	**149.5**	**401.7**	**551.9**	**208.2**
Eu*/Eu	**0.64**	**0.68**	**0.66**	**0.69**	**0.62**	**0.64**	**0.64**	**0.58**	**0.65**	**0.65**	**0.69**	**0.67**	**0.64**	**0.59**	**0.67**
Ce^{4+}/Ce^{3+}	**1400**	**2885**	**708.4**	**6296**	**1433**	**1235**	**758.6**	**4828**	**992.5**	**1545**	**700.1**	**811.2**	**1628**	**4175**	**585.3**
Yb/Gd	**12.78**	**13.61**	**20.38**	**30.49**	**17.71**	**18.47**	**21.73**	**19.40**	**17.01**	**16.50**	**22.00**	**21.28**	**20.17**	**15.17**	**19.75**
T_{Ti}(ºC)	**550.1**	**644.7**	**642.2**	**528.7**	**550.5**	**604.1**	**496.3**	**559.9**	**594.1**	**557.7**	**572.6**	**512.9**	**508.0**	**513.2**	**551.7**
$\log fO_2$	**-13.0**	**-3.8**	**-9.2**	**-9.1**	**-12.9**	**-9.6**	**-19.7**	**-7.6**	**-11.1**	**-12.1**	**-13.9**	**-18.1**	**-15.9**	**-11.9**	**-16.2**

701 **Table 4 Hf isotopic compositions of zircons from the syenite and the pegmatite**

702

Spots	Age /Ma	$^{176}Hf/^{177}Hf$	±2σ	$^{176}Yb/^{177}Hf$	$^{176}Lu/^{177}Hf$	fLu/Hf	$\varepsilon_{Hf}(0)$	$\varepsilon_{Hf}(t)$	T_{DM}(Ma)	T^{C}_{DM}(Ma)
Zircons from the syenite										
T37-1	31.2	0.282777	0.000008	0.02700	0.00091	-0.9726	0.2	0.8	671.4	1056.9
T37-3	31.2	0.282783	0.000001	0.00715	0.00026	-0.9922	0.4	1.1	651.3	1040.8
T37-8	31.2	0.282764	0.000013	0.01279	0.00043	-0.9869	-0.3	0.4	681.3	1085.7
T37-9	31.2	0.282785	0.000006	0.01041	0.00036	-0.9892	0.5	1.1	650.7	1038.6
T37-10	31.2	0.282785	0.000012	0.03536	0.00114	-0.9656	0.5	1.2	664.5	1038.4
T37-11	31.2	0.282782	0.000002	0.01359	0.00049	-0.9853	0.3	1.1	657.4	1044.8
T37-14	31.2	0.282758	0.000003	0.02874	0.00092	-0.9721	-0.5	0.2	699.2	1100.7
T37-15	31.2	0.282800	0.000003	0.00447	0.00016	-0.9952	1.0	1.7	626.5	1003.9
T37-17	31.2	0.282796	0.000003	0.01502	0.00053	-0.9841	0.8	1.5	639.0	1014.9
T37-18	31.2	0.282783	0.000025	0.03128	0.00106	-0.9681	0.4	1.1	665.5	1042.2
T37-19	31.2	0.282817	0.000001	0.01645	0.00056	-0.9830	1.6	2.3	609.9	965.5
T37-20	31.2	0.282769	0.000001	0.00895	0.00032	-0.9905	-0.1	0.6	672.0	1074.4
T37-21	31.2	0.282763	0.000004	0.02655	0.00099	-0.9701	-0.3	0.4	692.7	1087.2
T37-22	31.2	0.282780	0.000013	0.00889	0.00031	-0.9908	0.3	0.9	657.5	1051.2
T37-24	31.2	0.282796	0.000002	0.02156	0.00075	-0.9774	0.8	1.5	642.1	1013.3
T25-13	31.2	0.282798	0.000001	0.00264	0.00010	-0.9971	0.9	1.6	628.9	1008.4
T25-18	31.2	0.282768	0.000001	0.01541	0.00053	-0.9842	-0.1	0.6	677.5	1075.8
T25-14	31.2	0.282785	0.000002	0.01622	0.00058	-0.9826	0.5	1.2	654.6	1038.1
T29-22	31.2	0.282806	0.000003	0.00722	0.00026	-0.9922	1.2	1.9	620.4	991.2
T29-14	31.2	0.282780	0.000001	0.00549	0.00020	-0.9940	0.3	0.9	655.0	1050.3
Zircons from the pegmatite										
T16-1	30.1	0.282785	0.000012	0.11474	0.00383	-0.8847	0.5	1.1	715.0	1041.4
T16-2	30.1	0.282772	0.000006	0.11516	0.00480	-0.8555	0.0	0.6	736.4	1072.9
T16-4	30.1	0.282827	0.000014	0.12587	0.00422	-0.8728	1.9	2.5	658.9	948.0
T16-5	30.1	0.282787	0.000036	0.11408	0.00489	-0.8528	0.5	1.0	735.2	1042.1
T16-6	30.1	0.282801	0.000002	0.00619	0.00020	-0.9938	1.0	1.7	625.8	1002.8

T16-8	**30.1**	**0.282786**	**0.000033**	**0.09064**	**0.00390**	**-0.8825**	**0.5**	**1.1**	**715.3**	**1040.2**
T37-1	**30.1**	**0.282805**	**0.000000**	**0.00617**	**0.00022**	**-0.9934**	**1.2**	**1.8**	**621.2**	**994.5**
T37-2	**30.1**	**0.282771**	**0.000001**	**0.00599**	**0.00021**	**-0.9936**	**0.0**	**0.6**	**667.9**	**1071.0**
T11-15	**30.1**	**0.282795**	**0.000039**	**0.05361**	**0.00211**	**-0.9365**	**0.8**	**1.4**	**667.8**	**1019.5**
T3-4	**30.1**	**0.282775**	**0.000022**	**0.02808**	**0.00124**	**-0.9628**	**0.1**	**0.8**	**679.7**	**1061.7**
T16-16	**30.1**	**0.282788**	**0.000001**	**0.09710**	**0.00331**	**-0.9003**	**0.6**	**1.2**	**700.1**	**1033.7**
T16-17	**30.1**	**0.282770**	**0.000003**	**0.09431**	**0.00314**	**-0.9054**	**-0.1**	**0.6**	**723.6**	**1074.0**
T16-18	**30.1**	**0.282760**	**0.000030**	**0.05606**	**0.00240**	**-0.9277**	**-0.4**	**0.2**	**724.0**	**1096.7**
T16-19	**30.1**	**0.282764**	**0.000004**	**0.02477**	**0.00092**	**-0.9723**	**-0.3**	**0.4**	**690.2**	**1085.8**

703

704

705 **Table 5 Major and trace elemental compositions of chevkinite from the pegmatite.**

706

	Core (Dark Zone)										
Spots	**T11-1**	**T11-2**	**T11-3**	**T12-1**	**T12-3**	**T12-4**	**T13-1**	**T13-2**	**T16-1**	**T16-2**	**T29-1**
SiO_2	**19.72**	**19.07**	**19.19**	**19.19**	**19.36**	**19.45**	**19.14**	**19.44**	**19.35**	**19.13**	**19.13**
TiO_2	**18.25**	**17.06**	**17.14**	**16.40**	**17.29**	**17.03**	**17.07**	**16.56**	**17.13**	**16.90**	**17.50**
Al_2O_3	**0.16**	**0.09**	**0.07**	**0.10**	**0.08**	**0.19**	**0.19**	**0.15**	**0.18**	**0.16**	**0.07**
FeO	**12.15**	**13.35**	**13.14**	**13.12**	**12.96**	**12.95**	**13.07**	**12.99**	**12.93**	**12.70**	**12.42**
MnO	**0.02**	**0.01**	**0.00**	**0.00**	**0.00**	**0.00**	**0.02**	**0.00**	**0.00**	**0.00**	**0.03**
MgO	**0.31**	**0.29**	**0.29**	**0.29**	**0.25**	**0.36**	**0.30**	**0.31**	**0.30**	**0.27**	**0.29**
CaO	**3.23**	**2.20**	**2.61**	**2.17**	**2.62**	**2.73**	**2.77**	**2.73**	**2.78**	**2.14**	**2.53**
SrO	**0.30**	**0.19**	**0.21**	**0.11**	**0.23**	**0.30**	**0.23**	**0.23**	**0.37**	**0.21**	**0.27**
ThO_2	**1.14**	**1.62**	**1.58**	**1.57**	**1.48**	**1.35**	**1.31**	**1.35**	**1.35**	**1.73**	**1.60**
La_2O_3	**8.40**	**9.45**	**8.57**	**9.20**	**9.03**	**8.59**	**8.66**	**8.58**	**8.85**	**8.95**	**8.84**
Ce_2O_3	**24.31**	**24.29**	**24.22**	**24.25**	**24.40**	**24.63**	**24.12**	**24.59**	**23.57**	**24.94**	**24.34**
Pr_2O_3	**3.06**	**3.05**	**3.13**	**3.33**	**3.31**	**3.35**	**3.24**	**3.01**	**3.13**	**3.11**	**3.19**
Nd_2O_3	**4.87**	**4.79**	**4.86**	**4.78**	**4.92**	**4.55**	**4.77**	**4.87**	**4.66**	**4.85**	**4.40**
Sm_2O_3	**0.25**	**0.23**	**0.07**	**0.36**	**0.13**	**0.06**	**0.22**	**0.23**	**0.27**	**0.31**	**0.39**
Gd_2O_3	**0.82**	**0.75**	**0.72**	**0.78**	**0.65**	**0.74**	**0.63**	**0.64**	**0.83**	**0.74**	**0.77**
Y_2O_3	**0.06**	**0.10**	**0.08**	**0.09**	**0.10**	**0.03**	**0.09**	**0.08**	**0.10**	**0.04**	**0.08**
ZrO_2	**0.14**	**0.11**	**0.16**	**0.16**	**0.19**	**0.09**	**0.18**	**0.21**	**0.12**	**0.07**	**0.10**
Nb_2O_5	**0.14**	**0.11**	**0.16**	**0.16**	**0.19**	**0.09**	**0.18**	**0.21**	**0.12**	**0.07**	**0.10**
Total	**97.33**	**96.73**	**96.21**	**96.04**	**97.18**	**96.48**	**96.17**	**96.17**	**96.01**	**96.30**	**96.02**
Structural Formula based on 22 oxygen											
La	**0.65**	**0.75**	**0.68**	**0.74**	**0.71**	**0.68**	**0.69**	**0.68**	**0.70**	**0.71**	**0.70**
Ce	**1.86**	**1.91**	**1.90**	**1.93**	**1.90**	**1.93**	**1.90**	**1.94**	**1.85**	**1.97**	**1.92**
Pr	**0.23**	**0.24**	**0.25**	**0.26**	**0.26**	**0.26**	**0.25**	**0.24**	**0.24**	**0.25**	**0.25**
Nd	**0.36**	**0.37**	**0.37**	**0.37**	**0.37**	**0.35**	**0.37**	**0.37**	**0.36**	**0.37**	**0.34**
Sm	**0.02**	**0.02**	**0.01**	**0.03**	**0.01**	**0.00**	**0.02**	**0.02**	**0.02**	**0.02**	**0.03**
Gd	**0.06**	**0.05**	**0.05**	**0.06**	**0.05**	**0.05**	**0.04**	**0.05**	**0.06**	**0.05**	**0.05**
Y	**0.01**	**0.01**	**0.01**	**0.01**	**0.01**	**0.00**	**0.01**	**0.01**	**0.01**	**0.00**	**0.01**

Ca	**0.72**	**0.51**	**0.60**	**0.50**	**0.60**	**0.63**	**0.64**	**0.63**	**0.64**	**0.50**	**0.58**
Th	**0.05**	**0.08**	**0.08**	**0.08**	**0.07**	**0.07**	**0.06**	**0.07**	**0.07**	**0.08**	**0.08**
Sr	**0.04**	**0.02**	**0.03**	**0.01**	**0.03**	**0.04**	**0.03**	**0.03**	**0.05**	**0.03**	**0.03**
Sum A	**4.01**	**3.96**	**3.97**	**3.98**	**4.01**	**4.00**	**4.00**	**4.02**	**3.99**	**4.00**	**3.99**
Fe+2	**1.00**	**1.00**	**1.00**	**1.00**	**1.00**	**1.00**	**1.00**	**1.00**	**1.00**	**1.00**	**1.00**
Mn	**0.00**	**0.00**	**0.00**	**0.00**	**0.00**	**0.00**	**0.00**	**0.00**	**0.00**	**0.00**	**0.00**
Sum B	**1.00**	**1.00**	**1.00**	**1.00**	**1.00**	**1.00**	**1.00**	**1.00**	**1.00**	**1.00**	**1.00**
Fe+2	**1.13**	**1.40**	**1.36**	**1.38**	**1.31**	**1.31**	**1.35**	**1.34**	**1.32**	**1.30**	**1.23**
Ti	**0.87**	**0.76**	**0.77**	**0.68**	**0.77**	**0.73**	**0.76**	**0.68**	**0.76**	**0.75**	**0.83**
Mg	**0.10**	**0.09**	**0.09**	**0.09**	**0.08**	**0.11**	**0.10**	**0.10**	**0.10**	**0.09**	**0.09**
Nb	**0.00**	**0.00**	**0.00**	**0.00**	**0.00**	**0.00**	**0.00**	**0.00**	**0.00**	**0.00**	**0.00**
Al	**0.04**	**0.02**	**0.02**	**0.03**	**0.02**	**0.05**	**0.05**	**0.04**	**0.04**	**0.04**	**0.02**
Zr	**0.01**	**0.01**	**0.02**	**0.02**	**0.02**	**0.01**	**0.02**	**0.02**	**0.01**	**0.01**	**0.01**
Sum C	**2.16**	**2.29**	**2.26**	**2.20**	**2.20**	**2.22**	**2.27**	**2.17**	**2.23**	**2.18**	**2.19**
Ti	**2.00**	**2.00**	**2.00**	**2.00**	**2.00**	**2.00**	**2.00**	**2.00**	**2.00**	**2.00**	**2.00**
Sum D	**2.00**	**2.00**	**2.00**	**2.00**	**2.00**	**2.00**	**2.00**	**2.00**	**2.00**	**2.00**	**2.00**
Si	**4.13**	**4.10**	**4.12**	**4.16**	**4.12**	**4.15**	**4.11**	**4.18**	**4.15**	**4.14**	**4.12**
Sum T	**4.13**	**4.10**	**4.12**	**4.16**	**4.12**	**4.15**	**4.11**	**4.18**	**4.15**	**4.14**	**4.12**
Cation Sum	**13.30**	**13.35**	**13.36**	**13.34**	**13.33**	**13.37**	**13.38**	**13.37**	**13.37**	**13.31**	**13.30**
$(Ca,Sr)_A$+(Ti,Zr)c	**1.65**	**1.30**	**1.41**	**1.21**	**1.41**	**1.41**	**1.44**	**1.36**	**1.46**	**1.28**	**1.46**
$(REE,Y)_A$+(M+2,+3)c	**4.32**	**4.75**	**4.63**	**4.77**	**4.62**	**4.58**	**4.62**	**4.63**	**4.55**	**4.68**	**4.53**
Li	**4.27**	**3.99**	**4.99**	**4.76**	**2.81**	**4.63**	**3.03**	**3.10**	**3.71**	**3.93**	**2.30**
Be	**0.43**	**0.94**	**1.08**	**0.44**	**0.65**	**0.66**	**0.96**	**0.95**	**0.45**	**1.00**	**0.97**
B	**6.40**	**7.79**	**3.46**	**4.34**	**3.09**	**6.82**	**5.95**	**3.39**	**4.42**	**5.42**	**5.29**
Sc	**5.10**	**15.6**	**5.41**	**6.03**	**9.43**	**8.65**	**13.0**	**10.9**	**10.7**	**5.41**	**7.21**
V	**333**	**423**	**323**	**329**	**400**	**364**	**405**	**376**	**367**	**355**	**337**
Cr	**7.26**	**32.7**		**0.83**	**2.57**	**3.72**	**38.4**		**9.92**	**0.73**	**0.082**
Co	**8.10**	**7.87**	**9.04**	**8.53**	**10.7**	**9.88**	**9.55**	**9.47**	**9.51**	**7.25**	**6.56**
Ni	**1.35**	**0.94**	**0.80**	**2.65**	**2.01**	**1.29**	**1.65**	**2.22**	**1.80**	**0.20**	**1.27**
Cu	**6.33**	**6.97**	**5.23**	**6.08**	**5.77**	**6.15**	**6.57**	**5.25**	**7.21**	**6.11**	**5.25**
Zn	**94.2**	**107**	**106**	**117**	**107**	**117**	**113**	**113**	**114**	**135**	**112**
Ga	**509**	**505**	**510**	**512**	**523**	**522**	**505**	**508**	**509**	**499**	**486**
Ge	**896**	**846**	**869**	**863**	**901**	**934**	**890**	**906**	**924**	**919**	**941**

Rb	**0.20**	**0.74**	**0.12**		**0.29**	**0.32**	**0.06**		**0.18**		**0.21**
Sr	**2510**	**2462**	**2144**	**2827**	**2854**	**2472**	**2744**	**3006**	**2845**	**2847**	**2625**
Y	**1465**	**639**	**1455**	**1287**	**978**	**1272**	**746**	**838**	**856**	**1232**	**1076**
Zr	**2314**	**558**	**1545**	**1275**	**812**	**1030**	**462**	**333**	**293**	**1105**	**1035**
Nb	**2880**	**2702**	**2922**	**2241**	**3380**	**3352**	**3454**	**3143**	**3150**	**2219**	**3007**
Mo	**0.38**	**1.26**	**1.10**	**0.79**	**0.71**	**0.59**	**0.74**	**1.13**	**0.25**	**1.05**	**1.08**
Cd	**0.28**	**0.22**	**0.34**	**0.14**	**0.27**	**0.07**	**0.19**	**0.18**	**0.061**		**0.18**
In	**0.25**	**0.24**	**0.24**	**0.22**	**0.34**	**0.31**	**0.28**	**0.27**	**0.34**	**0.14**	**0.24**
Sn	**21.3**	**12.0**	**11.5**	**11.7**	**11.6**	**10.7**	**8.19**	**8.23**	**8.30**	**11.2**	**15.6**
Sb	**0.92**	**1.13**	**0.72**	**1.00**	**0.88**	**0.77**	**1.00**	**0.95**	**0.92**	**0.72**	**0.86**
Cs		**0.05**	**0.01**	**0.00**	**0.08**	**0.07**	**0.30**	**0.05**			**0.04**
Ba	**15.6**	**19.3**	**15.0**	**41.1**	**17.3**	**15.8**	**19.3**	**22.4**	**19.5**	**41.9**	**22.6**
La	**85296**	**96460**	**87894**	**88030**	**85190**	**85845**	**91907**	**91483**	**91027**	**93088**	**91718**
Ce	**189055**	**200768**	**194700**	**194475**	**200434**	**199641**	**201569**	**199360**	**200616**	**196709**	**196701**
Pr	**21978**	**21736**	**22013**	**22085**	**23171**	**22683**	**22243**	**22306**	**22414**	**21847**	**21955**
Nd	**74292**	**68702**	**77104**	**76928**	**82679**	**79926**	**75289**	**76587**	**77988**	**75628**	**74897**
Sm	**7867**	**5996**	**8008**	**7949**	**8440**	**8379**	**7136**	**7616**	**7654**	**7603**	**7341**
Eu	**1253**	**899**	**1261**	**1231**	**1289**	**1317**	**1093**	**1193**	**1232**	**1209**	**1200**
Gd	**2721**	**1881**	**2759**	**2745**	**2754**	**2868**	**2356**	**2568**	**2647**	**2804**	**2733**
Tb	**197**	**119**	**196**	**189**	**175**	**191**	**142**	**156**	**157**	**181**	**170**
Dy	**603**	**307**	**585**	**529**	**442**	**527**	**361**	**407**	**417**	**533**	**506**
Ho	**72.1**	**33.9**	**71.9**	**65.2**	**50.0**	**62.9**	**38.8**	**43.2**	**45.1**	**60.9**	**56.3**
Er	**192**	**92.7**	**192**	**167**	**131**	**176**	**108**	**120**	**122**	**170**	**151**
Tm	**26.5**	**11.4**	**27.7**	**24.1**	**17.9**	**25.0**	**12.8**	**13.4**	**13.6**	**21.1**	**17.2**
Yb	**178**	**74.5**	**187**	**164**	**150**	**188**	**95.6**	**99.5**	**100**	**150**	**114**
Lu	**38.7**	**17.6**	**42.3**	**38.9**	**37.2**	**45.9**	**23.6**	**22.6**	**24.0**	**34.1**	**25.2**
Hf	**84.2**	**18.3**	**59.2**	**46.5**	**40.1**	**40.3**	**20.1**	**19.0**	**15.0**	**35.7**	**41.2**
Ta	**64.8**	**55.3**	**69.2**	**52.1**	**48.7**	**55.4**	**46.3**	**60.7**	**58.1**	**47.7**	**63.2**
W	**93.5**	**78.7**	**92.9**	**75.4**	**139**	**130**	**114**	**112**	**131**	**76.5**	**77.1**
Bi	**27.2**	**12.6**	**27.2**	**30.3**	**10.9**	**15.8**	**13.7**	**5.31**	**5.91**	**27.5**	**27.5**
Pb	**486.4**	**353.5**	**426.6**	**581.0**	**342.4**	**377.2**	**329.2**	**262.8**	**314.1**	**532.4**	**453.8**
Th	**13888**	**9755**	**17288**	**16979**	**9692**	**11879**	**10382**	**9153**	**9523**	**17089**	**14419**
U	**475**	**386**	**522**	**502**	**267**	**398**	**292**	**269**	**282**	**492**	**358**

707

708

	Rim (lighter Zone)									
Spots	**T11-1**	**T11-2**	**T11-3**	**T12-1**	**T12-3**	**T12-4**	**T13-1**	**T13-2**	**T16-1**	**T16-2**
SiO_2	**19.22**	**18.69**	**19.11**	**18.98**	**18.96**	**19.03**	**19.02**	**19.05**	**18.89**	**19.26**
TiO_2	**16.13**	**16.99**	**16.42**	**16.22**	**16.57**	**15.89**	**16.50**	**16.19**	**16.15**	**17.74**
Al_2O_3	**0.12**	**0.08**	**0.16**	**0.10**	**0.17**	**0.15**	**0.17**	**0.14**	**0.15**	**0.08**
FeO	**13.42**	**12.82**	**12.94**	**13.36**	**13.11**	**13.04**	**13.13**	**13.31**	**13.28**	**12.68**
MnO	**0.023**	**0.00**	**0.00**	**0.02**	**0.00**	**0.00**	**0.00**	**0.01**	**0.00**	**0.00**
MgO	**0.32**	**0.29**	**0.30**	**0.33**	**0.30**	**0.27**	**0.33**	**0.32**	**0.29**	**0.30**
CaO	**1.88**	**1.30**	**1.93**	**1.78**	**1.96**	**1.76**	**1.88**	**1.82**	**1.87**	**1.79**
SrO	**0.23**	**0.19**	**0.19**	**0.13**	**0.13**	**0.15**	**0.21**	**0.16**	**0.27**	**0.34**
ThO_2	**2.80**	**0.46**	**2.52**	**2.68**	**2.14**	**2.31**	**2.57**	**2.64**	**2.76**	**2.80**
La_2O_3	**9.55**	**9.61**	**9.06**	**9.42**	**9.30**	**8.98**	**9.29**	**9.42**	**9.29**	**8.81**
Ce_2O_3	**24.27**	**26.47**	**25.72**	**25.45**	**24.15**	**24.95**	**25.27**	**25.36**	**25.95**	**23.66**
Pr_2O_3	**3.37**	**3.28**	**3.18**	**3.36**	**3.49**	**3.37**	**3.29**	**3.15**	**3.52**	**3.12**
Nd_2O_3	**4.51**	**5.13**	**4.63**	**4.96**	**4.78**	**4.92**	**4.42**	**4.67**	**4.43**	**4.51**
Sm_2O_3	**0.18**	**0.22**	**0.24**	**0.19**	**0.18**	**0.21**	**0.14**	**0.23**	**0.08**	**0.24**
Gd_2O_3	**0.86**	**0.71**	**0.80**	**0.71**	**0.77**	**0.77**	**0.76**	**0.69**	**0.68**	**0.75**
Y_2O_3	**0.04**	**0.07**	**0.10**	**0.02**	**0.05**	**0.04**	**0.04**	**0.01**	**0.04**	**0.12**
ZrO_2	**0.08**	**0.04**	**0.09**	**0.05**	**0.08**	**0.00**	**0.03**	**0.06**	**0.09**	**0.24**
Nb_2O_5	**0.45**	**0.37**	**0.32**	**0.34**	**0.46**	**0.47**	**0.41**	**0.45**	**0.48**	**0.42**
Total	**97.45**	**96.72**	**97.70**	**98.08**	**96.59**	**96.30**	**97.44**	**97.65**	**98.22**	**96.85**
Structural Formula based on 22 oxygen										
La	**0.76**	**0.77**	**0.72**	**0.75**	**0.74**	**0.73**	**0.74**	**0.75**	**0.74**	**0.70**
Ce	**1.92**	**2.11**	**2.03**	**2.01**	**1.92**	**2.00**	**2.00**	**2.01**	**2.06**	**1.85**
Pr	**0.27**	**0.26**	**0.25**	**0.26**	**0.28**	**0.27**	**0.26**	**0.25**	**0.28**	**0.24**
Nd	**0.35**	**0.40**	**0.36**	**0.38**	**0.37**	**0.39**	**0.34**	**0.36**	**0.34**	**0.34**
Sm	**0.01**	**0.02**	**0.02**	**0.01**	**0.01**	**0.02**	**0.01**	**0.02**	**0.01**	**0.02**
Gd	**0.06**	**0.05**	**0.06**	**0.05**	**0.06**	**0.06**	**0.05**	**0.05**	**0.05**	**0.05**
Y	**0.00**	**0.01**	**0.01**	**0.00**	**0.01**	**0.00**	**0.00**	**0.00**	**0.00**	**0.01**
Ca	**0.44**	**0.30**	**0.45**	**0.41**	**0.46**	**0.41**	**0.43**	**0.42**	**0.43**	**0.41**

Th	**0.14**	**0.02**	**0.12**	**0.13**	**0.11**	**0.12**	**0.13**	**0.13**	**0.14**	**0.14**
Sr	**0.03**	**0.02**	**0.02**	**0.02**	**0.02**	**0.02**	**0.03**	**0.02**	**0.03**	**0.04**
Sum A	**3.98**	**3.97**	**4.04**	**4.04**	**3.96**	**4.00**	**4.00**	**4.01**	**4.08**	**3.81**
Fe+2	**1.00**	**1.00**	**1.00**	**1.00**	**1.00**	**1.00**	**1.00**	**1.00**	**1.00**	**1.00**
Mn	**0.00**	**0.00**	**0.00**	**0.00**	**0.00**	**0.00**	**0.00**	**0.00**	**0.00**	**0.00**
Sum B	**1.00**	**1.00**	**1.00**	**1.00**	**1.00**	**1.00**	**1.00**	**1.00**	**1.00**	**1.00**
Fe+2	**1.43**	**1.33**	**1.33**	**1.42**	**1.38**	**1.39**	**1.37**	**1.41**	**1.40**	**1.27**
Ti	**0.62**	**0.78**	**0.66**	**0.64**	**0.70**	**0.62**	**0.68**	**0.64**	**0.63**	**0.86**
Mg	**0.10**	**0.09**	**0.10**	**0.11**	**0.10**	**0.09**	**0.10**	**0.10**	**0.09**	**0.09**
Nb	**0.01**	**0.01**	**0.01**	**0.01**	**0.01**	**0.01**	**0.01**	**0.01**	**0.01**	**0.01**
Al	**0.03**	**0.02**	**0.04**	**0.03**	**0.04**	**0.04**	**0.04**	**0.03**	**0.04**	**0.02**
Zr	**0.01**	**0.00**	**0.01**	**0.00**	**0.01**	**0.00**	**0.00**	**0.01**	**0.01**	**0.02**
Sum C	**2.20**	**2.24**	**2.15**	**2.20**	**2.24**	**2.14**	**2.21**	**2.20**	**2.18**	**2.27**
Ti	**2.00**	**2.00**	**2.00**	**2.00**	**2.00**	**2.00**	**2.00**	**2.00**	**2.00**	**2.00**
Sum D	**2.00**	**2.00**	**2.00**	**2.00**	**2.00**	**2.00**	**2.00**	**2.00**	**2.00**	**2.00**
Si	**4.16**	**4.07**	**4.12**	**4.10**	**4.11**	**4.17**	**4.11**	**4.12**	**4.09**	**4.12**
Sum T	**4.16**	**4.07**	**4.12**	**4.10**	**4.11**	**4.17**	**4.11**	**4.12**	**4.09**	**4.12**
Cation Sum	**13.34**	**13.28**	**13.31**	**13.34**	**13.32**	**13.31**	**13.32**	**13.33**	**13.35**	**13.21**
$(Ca,Sr)_A+(Ti,Zr)c$	**1.10**	**1.11**	**1.14**	**1.07**	**1.18**	**1.05**	**1.14**	**1.08**	**1.10**	**1.33**
$(REE,Y)_A+(M+2,+3)c$	**4.80**	**4.95**	**4.78**	**4.90**	**4.76**	**4.85**	**4.78**	**4.85**	**4.88**	**4.49**
Li	**5.92**	**5.92**	**4.97**	**7.67**	**6.05**	**5.90**	**4.92**	**6.39**	**4.73**	**3.90**
Be	**0.31**	**1.25**	**0.94**	**0.11**	**0.63**	**0.63**	**0.32**	**1.13**	**0.80**	**1.31**
B	**4.86**	**5.92**	**3.64**	**3.45**	**4.17**	**3.75**	**1.64**	**6.69**	**4.01**	**3.92**
Sc	**4.20**	**5.28**	**5.78**	**6.87**	**6.04**	**6.22**	**5.22**	**6.18**	**8.03**	**3.74**
V	**357**	**336**	**338**	**335**	**335**	**346**	**344**	**328**	**342**	**321**
Cr	**12.8**	**3.73**	**11.5**		**12.8**	**3.11**	**1.31**	**2.26**	**6.87**	
Co	**7.70**	**8.36**	**9.03**	**9.66**	**10.5**	**8.92**	**7.57**	**9.17**	**9.14**	**7.82**
Ni	**0.99**	**1.54**	**1.88**	**0.94**	**1.46**	**1.68**	**0.75**	**2.24**	**1.46**	**1.66**
Cu	**6.33**	**5.08**	**6.16**	**5.56**	**7.85**	**5.93**	**5.56**	**6.65**	**15.4**	**5.66**
Zn	**112**	**111**	**112**	**126**	**135**	**134**	**127**	**132**	**138**	**134**
Ga	**513**	**511**	**509**	**503**	**498**	**508**	**489**	**503**	**500**	**489**
Ge	**873**	**898**	**858**	**828**	**869**	**882**	**862**	**847**	**927**	**942**
Rb		**0.19**	**0.08**	**0.11**	**0.07**		**0.05**	**0.58**	**0.24**	**0.14**

Sr	**2211**	**2461**	**2667**	**2428**	**2087**	**1790**	**2532**	**1976**	**2651**	**1988**
Y	**1086**	**1291**	**1051**	**1164**	**1139**	**1326**	**1119**	**1343**	**972**	**1490**
Zr	**732**	**1106**	**978**	**850**	**619**	**513**	**918**	**1050**	**622**	**1161**
Nb	**2836**	**2442**	**2320**	**2331**	**2306**	**2377**	**2497**	**2832**	**2713**	**2628**
Mo	**0.58**	**0.99**	**0.18**	**0.66**	**0.95**	**0.58**	**0.80**	**0.46**	**1.29**	**0.97**
Cd		**0.28**	**0.14**	**0.21**	**0.06**	**0.06**	**0.04**	**0.05**	**0.02**	
In	**0.14**	**0.15**	**0.29**	**0.18**	**0.18**	**0.29**	**0.16**	**0.29**	**0.30**	**0.17**
Sn	**7.64**	**8.79**	**7.69**	**6.24**	**6.42**	**5.71**	**7.43**	**9.41**	**6.94**	**10.5**
Sb	**0.61**	**0.70**	**1.10**	**1.09**	**0.86**	**0.76**	**1.06**	**0.88**	**1.61**	**0.79**
Cs		**0.06**	**0.04**				**0.04**	**0.03**	**0.03**	
Ba	**15.8**	**18.3**	**30.2**	**23.1**	**15.0**	**12.4**	**26.7**	**21.7**	**21.7**	**13.4**
La	**89676**	**83439**	**88589**	**87142**	**87815**	**87347**	**92387**	**89411**	**93700**	**92673**
Ce	**196249**	**189610**	**194208**	**191891**	**193497**	**195218**	**195860**	**195571**	**198446**	**196758**
Pr	**22223**	**22057**	**21959**	**21720**	**21657**	**22054**	**21534**	**21527**	**21957**	**21896**
Nd	**73973**	**75648**	**74649**	**75256**	**74847**	**78297**	**73754**	**76601**	**74584**	**75013**
Sm	**7331**	**7831**	**7316**	**7565**	**7504**	**8214**	**7232**	**7782**	**7243**	**7693**
Eu	**1121**	**1223**	**1079**	**1155**	**1174**	**1283**	**1145**	**1229**	**1143**	**1279**
Gd	**2444**	**2678**	**2409**	**2540**	**2680**	**2847**	**2638**	**2791**	**2594**	**2997**
Tb	**167**	**190**	**163**	**175**	**173**	**201**	**169**	**187**	**159**	**198**
Dy	**475**	**551**	**445**	**484**	**496**	**568**	**492**	**552**	**448**	**629**
Ho	**54.4**	**65.0**	**52.1**	**57.7**	**57.9**	**67.7**	**55.8**	**66.2**	**49.2**	**71.5**
Er	**142**	**165**	**139**	**156**	**150**	**161**	**154**	**176**	**136**	**200**
Tm	**18.6**	**22.6**	**20.5**	**20.7**	**17.9**	**19.5**	**19.0**	**23.5**	**17.2**	**25.8**
Yb	**123**	**148**	**150**	**145**	**126**	**128**	**130**	**162**	**114**	**162**
Lu	**28.1**	**33.9**	**35.2**	**33.4**	**27.8**	**27.3**	**30.4**	**35.7**	**27.7**	**36.1**
Hf	**23.2**	**41.9**	**35.4**	**29.6**	**21.0**	**18.5**	**32.6**	**37.7**	**24.7**	**36.1**
Ta	**67.7**	**63.1**	**46.7**	**58.0**	**51.7**	**56.9**	**59.1**	**67.3**	**56.7**	**65.0**
W	**71.7**	**68.6**	**69.4**	**54.5**	**57.4**	**67.3**	**57.1**	**86.4**	**84.9**	**67.1**
Bi	**22.5**	**26.2**	**25.3**	**24.4**	**23.0**	**26.8**	**24.7**	**22.3**	**18.1**	**27.5**
Pb	**416.3**	**522.4**	**530.1**	**515.9**	**452.4**	**386.8**	**517.1**	**457.8**	**442.7**	**418.4**
Th	**20916**	**25079**	**22009**	**28414**	**24411**	**23110**	**25610**	**19822**	**18330**	**18420**
U	**591**	**773**	**536**	**802**	**681**	**742**	**701**	**557**	**413**	**631**

709

710

711 **Table 6 Major and trace elemental compositions of monazites from the pegmatite**

712

	Core										
Spots	**T20-6**	**T20-5**	**T20-1**	**T3-1**	**T3-2**	**T3-6**	**T3-5**	**T11b-4**	**T11b-5**	**T11b-6**	**T11b-8**
SiO_2	**1.24**	**1.11**	**1.15**	**1.25**	**1.20**	**1.17**	**1.24**	**1.19**	**1.20**	**1.15**	**1.13**
P_2O_5	**26.80**	**26.89**	**27.16**	**26.52**	**27.46**	**26.74**	**26.94**	**26.88**	**26.83**	**27.47**	**27.17**
CaO	**0.32**	**0.29**	**0.26**	**0.51**	**0.40**	**0.39**	**0.37**	**0.29**	**0.47**	**0.40**	**0.35**
SO_3	**0.79**	**0.67**	**0.74**	**1.15**	**0.97**	**0.88**	**0.94**	**0.87**	**0.96**	**0.96**	**0.88**
ThO_2	**1.50**	**1.52**	**1.56**	**1.25**	**1.18**	**1.19**	**1.19**	**1.35**	**1.18**	**1.22**	**1.14**
La_2O_3	**17.52**	**17.88**	**19.28**	**17.91**	**18.26**	**18.40**	**17.45**	**18.77**	**16.82**	**16.82**	**16.62**
Ce_2O_3	**38.47**	**37.91**	**37.49**	**38.21**	**38.18**	**38.16**	**38.17**	**37.18**	**38.50**	**38.18**	**38.72**
Pr_2O_3	**3.07**	**3.17**	**2.92**	**3.26**	**2.90**	**3.13**	**3.20**	**2.95**	**3.17**	**3.29**	**3.14**
Nd_2O_3	**10.88**	**10.51**	**10.40**	**9.63**	**10.31**	**9.93**	**10.70**	**10.09**	**10.72**	**10.59**	**10.67**
Total	**100.58**	**99.94**	**100.97**	**99.69**	**100.85**	**99.98**	**100.20**	**99.58**	**99.85**	**100.06**	**99.81**
Structural Formula Based on 4-Oxygen											
Si	**0.05**	**0.04**	**0.05**	**0.05**	**0.05**	**0.05**	**0.05**	**0.05**	**0.05**	**0.05**	**0.04**
P	**0.90**	**0.91**	**0.91**	**0.90**	**0.91**	**0.91**	**0.91**	**0.91**	**0.91**	**0.92**	**0.92**
Ca	**0.01**	**0.01**	**0.01**	**0.02**	**0.02**	**0.02**	**0.02**	**0.01**	**0.02**	**0.02**	**0.01**
S	**0.02**	**0.02**	**0.02**	**0.03**	**0.03**	**0.03**	**0.03**	**0.03**	**0.03**	**0.03**	**0.03**
Th	**0.01**	**0.01**	**0.01**	**0.01**	**0.01**	**0.01**	**0.01**	**0.01**	**0.01**	**0.01**	**0.01**
La	**0.26**	**0.26**	**0.28**	**0.26**	**0.26**	**0.27**	**0.26**	**0.28**	**0.25**	**0.24**	**0.24**
Ce	**0.56**	**0.56**	**0.54**	**0.56**	**0.55**	**0.56**	**0.56**	**0.54**	**0.56**	**0.55**	**0.56**
Pr	**0.04**	**0.05**	**0.04**	**0.05**	**0.04**	**0.05**	**0.05**	**0.04**	**0.05**	**0.05**	**0.05**
Nd	**0.15**	**0.15**	**0.15**	**0.14**	**0.14**	**0.14**	**0.15**	**0.14**	**0.15**	**0.15**	**0.15**
Cation Sum	**2.02**	**2.02**	**2.02**	**2.02**	**2.02**	**2.02**	**2.02**	**2.02**	**2.02**	**2.01**	**2.02**
(Y+REE)	**1.02**	**1.02**	**1.02**	**1.01**	**1.00**	**1.02**	**1.01**	**1.01**	**1.01**	**0.99**	**1.01**
Th+Si+Ca	**0.08**	**0.07**	**0.07**	**0.08**	**0.07**	**0.07**	**0.08**	**0.07**	**0.08**	**0.07**	**0.07**
REE+P	**1.92**	**1.93**	**1.93**	**1.90**	**1.91**	**1.92**	**1.92**	**1.92**	**1.91**	**1.91**	**1.92**
Th+Si	**0.06**	**0.06**	**0.06**	**0.06**	**0.06**	**0.06**	**0.06**	**0.06**	**0.06**	**0.06**	**0.06**

La	**146186**	**147462**	**154419**	**164840**	**146335**	**146335**	**168076**	**160136**	**159241**	**179849**	**174548**
Ce	**300587**	**301063**	**309872**	**323318**	**302227**	**302227**	**311546**	**304995**	**301069**	**341061**	**341790**
Pr	**31781**	**31504**	**32134**	**32867**	**32170**	**32170**	**31118**	**30670**	**30954**	**34667**	**34799**
Nd	**101237**	**100761**	**102403**	**102843**	**103091**	**103091**	**99075**	**97653**	**98267**	**108418**	**108835**
Sm	**8002**	**7894**	**7608**	**6819**	**8080**	**8080**	**6852**	**7078**	**7284**	**5256**	**5472**
Eu	**1026**	**1011**	**961.9**	**867.9**	**1011**	**1011**	**888.4**	**904.8**	**927.6**	**679.0**	**700.7**
Gd	**2837**	**2807**	**2658**	**2426**	**2807**	**2807**	**2481**	**2536**	**2612**	**1882**	**1936**
Tb	**133.4**	**133.7**	**126.1**	**113.2**	**130.3**	**130.3**	**118.0**	**121.1**	**123.8**	**89.35**	**91.24**
Dy	**231.6**	**228.9**	**217.0**	**190.6**	**223.4**	**223.4**	**206.2**	**209.2**	**217.0**	**154.5**	**160.0**
Ho	**18.93**	**18.46**	**16.90**	**15.55**	**18.33**	**18.33**	**16.90**	**16.84**	**16.81**	**12.40**	**12.58**
Er	**59.15**	**57.62**	**55.75**	**49.31**	**59.15**	**59.15**	**52.91**	**52.06**	**53.12**	**39.67**	**39.38**
Tm	**1.50**	**1.38**	**1.44**	**1.39**	**1.58**	**1.58**	**1.42**	**1.14**	**1.23**	**1.05**	**1.13**
Yb	**8.23**	**8.21**	**8.28**	**6.87**	**9.07**	**9.07**	**7.16**	**6.32**	**5.63**	**5.10**	**6.05**
Lu	**0.99**	**0.73**	**1.07**	**0.90**	**1.15**	**1.15**	**0.82**	**0.83**	**0.71**	**0.65**	**0.61**
Hf	**0.17**	**0.30**	**0.22**	**0.14**	**0.14**	**0.14**	**0.12**	**0.17**	**0.17**	**0.14**	**0.18**
Ta	**0.04**	**0.03**	**0.00**	**0.02**	**0.02**	**0.02**	**0.02**	**0.01**	**0.02**	**0.02**	**0.03**
Pb	**26.48**	**42.92**	**22.75**	**21.35**	**24.58**	**24.58**	**22.41**	**43.84**	**31.99**	**19.41**	**28.06**
Th	**10376**	**13457**	**10354**	**10934**	**10485**	**10485**	**10360**	**18789**	**13557**	**13648**	**13984**
U	**102.4**	**115.4**	**99.50**	**90.04**	**107.86**	**107.9**	**79.65**	**119.0**	**92.52**	**69.51**	**74.75**
Li	**5.13**	**7.99**	**5.94**	**3.60**	**2.09**	**2.09**	**8.25**	**6.15**	**4.71**	**2.59**	**3.78**
B	**2.97**	**1.51**	**1.29**	**1.04**	**1.96**	**1.96**	**2.11**	**1.66**	**1.56**	**1.37**	**1.09**
Sc	**0.00**	**0.93**	**0.00**	**0.00**	**0.00**	**0.00**	**0.00**	**0.00**	**1.22**	**0.01**	**0.00**
V	**28.40**	**24.62**	**28.03**	**25.10**	**27.43**	**27.43**	**24.48**	**23.26**	**27.24**	**20.64**	**18.51**
Cr	**1.40**	**5.47**	**0.00**	**0.04**	**1.70**	**1.70**	**0.00**	**0.00**	**3.36**	**0.61**	**0.00**
Ga	**755.4**	**732.3**	**703.2**	**637.2**	**754.1**	**754.1**	**658.7**	**681.7**	**722.7**	**497.3**	**506.7**
Ge	**1298**	**1235**	**1194**	**1084**	**1281**	**1281**	**1071**	**1130**	**1169**	**840.7**	**859.2**
Sr	**1015**	**598.0**	**864.9**	**722.0**	**910.9**	**910.9**	**931.0**	**736.5**	**668.3**	**573.0**	**588.4**
Y	**424.6**	**418.8**	**386.8**	**353.0**	**413.4**	**413.4**	**382.4**	**368.0**	**393.0**	**279.1**	**288.6**
Zr	**0.59**	**0.47**	**0.48**	**0.46**	**0.50**	**0.50**	**0.58**	**0.37**	**0.75**	**0.29**	**0.45**
Nb	**0.20**	**0.09**	**0.08**	**0.11**	**0.12**	**0.12**	**0.15**	**0.21**	**0.11**	**0.05**	**0.07**
Mo	**0.20**	**0.21**	**0.35**	**0.14**	**0.29**	**0.29**	**0.15**	**0.08**	**0.08**	**0.15**	**0.23**
Sn	**0.14**	**0.10**	**0.18**	**0.04**	**0.00**	**0.00**	**0.01**	**0.07**	**0.02**	**0.05**	**0.07**

Ba	**2.08**	**1.84**	**1.49**	**0.95**	**1.31**	**1.31**	**1.74**	**1.24**	**0.70**	**0.64**	**0.98**

713

	Outer Core										
Spots	**T20-6**	**T20-5**	**T20-1**	**T3-1**	**T3-2**	**T3-6**	**T3-5**	**T11b-4**	**T11b-5**	**T11b-6**	**T11b-8**
SiO_2	**1.50**	**1.45**	**1.58**	**1.62**	**1.53**	**1.22**	**1.44**	**1.55**	**1.48**	**1.45**	**1.32**
P_2O_5	**26.62**	**26.57**	**26.40**	**26.80**	**26.56**	**27.09**	**26.12**	**26.48**	**26.44**	**26.32**	**26.60**
CaO	**0.49**	**0.47**	**0.47**	**0.48**	**0.30**	**0.31**	**0.28**	**0.40**	**0.26**	**0.41**	**0.27**
SO_3	**1.19**	**1.12**	**1.11**	**1.23**	**1.22**	**0.78**	**0.79**	**1.00**	**1.20**	**1.07**	**1.01**
ThO_2	**2.49**	**2.48**	**2.55**	**2.42**	**2.27**	**1.46**	**1.75**	**2.29**	**1.77**	**2.42**	**1.76**
La_2O_3	**16.89**	**16.43**	**17.60**	**17.02**	**16.69**	**18.78**	**16.63**	**16.09**	**16.88**	**16.05**	**17.02**
Ce_2O_3	**37.49**	**37.68**	**37.54**	**36.92**	**38.25**	**37.83**	**38.16**	**37.65**	**38.00**	**37.54**	**39.04**
Pr_2O_3	**3.01**	**3.22**	**3.16**	**2.98**	**3.23**	**3.03**	**3.29**	**3.51**	**3.24**	**3.29**	**3.21**
Nd_2O_3	**10.46**	**10.63**	**10.17**	**10.35**	**10.67**	**10.14**	**10.62**	**10.91**	**10.52**	**11.06**	**10.74**
Total	**100.13**	**100.04**	**100.55**	**99.81**	**100.71**	**100.63**	**99.08**	**99.89**	**99.78**	**99.60**	**100.97**
Structural Formula Based on 4-Oxygen											
Si	**0.06**	**0.06**	**0.06**	**0.06**	**0.06**	**0.05**	**0.06**	**0.06**	**0.06**	**0.06**	**0.05**
P	**0.89**	**0.90**	**0.89**	**0.90**	**0.89**	**0.91**	**0.90**	**0.89**	**0.89**	**0.89**	**0.89**
Ca	**0.02**	**0.02**	**0.02**	**0.02**	**0.01**	**0.01**	**0.01**	**0.02**	**0.01**	**0.02**	**0.01**
S	**0.04**	**0.03**	**0.03**	**0.04**	**0.04**	**0.02**	**0.02**	**0.03**	**0.04**	**0.03**	**0.03**
Th	**0.02**	**0.02**	**0.02**	**0.02**	**0.02**	**0.01**	**0.02**	**0.02**	**0.02**	**0.02**	**0.02**
La	**0.25**	**0.24**	**0.26**	**0.25**	**0.24**	**0.27**	**0.25**	**0.24**	**0.25**	**0.24**	**0.25**
Ce	**0.54**	**0.55**	**0.55**	**0.53**	**0.55**	**0.55**	**0.57**	**0.55**	**0.55**	**0.55**	**0.57**
Pr	**0.04**	**0.05**	**0.05**	**0.04**	**0.05**	**0.04**	**0.05**	**0.05**	**0.05**	**0.05**	**0.05**
Nd	**0.15**	**0.15**	**0.14**	**0.15**	**0.15**	**0.14**	**0.15**	**0.16**	**0.15**	**0.16**	**0.15**
Cation Sum	**2.01**	**2.02**	**2.02**	**2.01**	**2.01**	**2.02**	**2.02**	**2.02**	**2.01**	**2.02**	**2.02**
(Y+REE)	**0.98**	**0.99**	**0.99**	**0.97**	**0.99**	**1.01**	**1.02**	**0.99**	**1.00**	**0.99**	**1.02**
Th+Si+Ca	**0.10**	**0.10**	**0.11**	**0.11**	**0.09**	**0.07**	**0.09**	**0.10**	**0.09**	**0.10**	**0.08**
REE+P	**1.88**	**1.88**	**1.88**	**1.87**	**1.88**	**1.92**	**1.91**	**1.89**	**1.89**	**1.89**	**1.91**
Th+Si	**0.08**	**0.08**	**0.09**	**0.09**	**0.08**	**0.06**	**0.07**	**0.08**	**0.08**	**0.08**	**0.07**

La	**137286**	**139704**	**142876**	**156119**	**141835**	**152952**	**164876**	**170806**	**168641**	**155680**	**108990**
Ce	**298553**	**298019**	**299650**	**314408**	**299413**	**269700**	**316817**	**322807**	**322811**	**295908**	**237773**
Pr	**32522**	**32049**	**32231**	**32940**	**32342**	**26294**	**30986**	**32718**	**33228**	**30479**	**25422**
Nd	**105471**	**103450**	**103248**	**106389**	**104748**	**84611**	**99714**	**103166**	**103726**	**96297**	**83167**
Sm	**8510**	**8073**	**8165**	**7375**	**8151**	**5896**	**6566**	**6411**	**6540**	**7213**	**6594**
Eu	**1074**	**1005**	**1026**	**919.5**	**1029**	**752.3**	**840.4**	**825.7**	**841.8**	**922.4**	**837.8**
Gd	**2924**	**2784**	**2838**	**2534**	**2816**	**2145**	**2347**	**2274**	**2352**	**2596**	**2279**
Tb	**139.7**	**127.1**	**132.4**	**119.1**	**134.3**	**104.8**	**112.1**	**109.0**	**114.2**	**124.3**	**108.7**
Dy	**237.1**	**211.8**	**226.4**	**212.4**	**229.9**	**191.6**	**197.3**	**189.3**	**200.9**	**220.8**	**188.1**
Ho	**18.65**	**17.05**	**18.71**	**17.00**	**18.36**	**15.16**	**16.00**	**14.75**	**15.20**	**17.88**	**14.55**
Er	**61.72**	**56.17**	**59.02**	**52.78**	**58.14**	**45.10**	**48.13**	**46.36**	**45.50**	**53.25**	**45.77**
Tm	**1.41**	**1.27**	**1.51**	**1.46**	**1.63**	**1.22**	**1.30**	**1.20**	**1.17**	**1.27**	**1.28**
Yb	**8.68**	**7.67**	**8.53**	**7.34**	**9.48**	**5.50**	**5.62**	**6.59**	**5.43**	**6.35**	**7.87**
Lu	**0.93**	**0.91**	**1.05**	**0.87**	**1.23**	**0.59**	**0.84**	**0.70**	**0.57**	**0.68**	**1.33**
Hf	**0.23**	**0.19**	**0.25**	**0.23**	**0.20**	**0.80**	**0.17**	**0.22**	**0.24**	**0.23**	**2.13**
Ta	**0.03**	**0.04**	**0.03**	**0.03**	**0.03**	**0.03**	**0.02**	**0.02**	**0.02**	**0.05**	**0.03**
Pb	**50.71**	**131.49**	**42.44**	**42.46**	**48.25**	**131.78**	**42.27**	**27.76**	**39.82**	**54.62**	**78.24**
Th	**20777**	**19014**	**17914**	**21802**	**20675**	**24506**	**21387**	**15080**	**19910**	**24786**	**16476**
U	**207.0**	**178.7**	**176.0**	**179.2**	**204.3**	**83.6**	**144.4**	**103.6**	**136.5**	**156.8**	**151.3**
Li	**5.24**	**4.34**	**4.26**	**3.46**	**6.73**	**18.21**	**5.72**	**4.87**	**6.56**	**5.28**	**17.06**
B	**2.61**	**1.89**	**2.39**	**2.00**	**0.22**	**1.59**	**0.26**	**1.43**	**0.96**	**2.07**	**1.91**
Sc	**0.00**	**0.00**	**0.03**	**0.00**	**0.05**	**1.97**	**0.02**	**0.68**	**0.00**	**0.30**	**7.76**
V	**26.97**	**25.19**	**29.06**	**24.19**	**29.35**	**55.81**	**23.67**	**19.68**	**17.11**	**27.62**	**121.28**
Cr	**0.27**	**0.18**	**0.00**	**0.00**	**8.88**	**0.00**	**0.73**	**1.02**	**0.54**	**1.01**	**9.37**
Ga	**750.2**	**745.8**	**751.6**	**654.1**	**737.9**	**585.2**	**617.5**	**597.3**	**588.6**	**700.1**	**586.7**
Ge	**1301.73**	**1243.50**	**1262**	**1107**	**1267**	**959.3**	**1040**	**992.4**	**1003**	**1165**	**1013**
Sr	**951.7**	**536.8**	**955.2**	**902.7**	**1021**	**346.8**	**877.1**	**812.3**	**505.6**	**653.6**	**605.4**
Y	**425.5**	**371.2**	**409.4**	**374.8**	**411.3**	**344.4**	**358.9**	**348.5**	**361.1**	**393.7**	**334.2**
Zr	**0.67**	**0.62**	**0.50**	**0.43**	**0.51**	**10.36**	**0.40**	**0.38**	**0.38**	**0.59**	**21.40**
Nb	**0.16**	**0.14**	**0.13**	**0.13**	**0.16**	**0.12**	**0.13**	**0.09**	**0.10**	**0.14**	**0.40**
Mo	**0.08**	**0.16**	**0.49**	**0.17**	**0.31**	**0.13**	**0.22**	**0.31**	**0.19**	**0.00**	**0.10**
Sn	**0.19**	**0.07**	**0.16**	**0.12**	**0.14**	**1.01**	**0.01**	**0.00**	**0.00**	**0.09**	**1.92**

Ba	**1.41**	**9.38**	**1.79**	**1.41**	**1.62**	**7.15**	**1.43**	**0.91**	**1.00**	**0.66**	**9.25**

714

	Rim										
Spots	**T20-6**	**T20-5**	**T20-1**	**T3-1**	**T3-2**	**T3-6**	**T3-5**	**T11b-4**	**T11b-5**	**T11b-6**	**T11b-8**
SiO_2	**1.30**	**1.50**	**1.37**	**1.58**	**1.77**	**1.54**	**1.51**	**1.31**	**1.53**	**1.08**	**1.10**
P_2O_5	**27.08**	**26.75**	**26.29**	**25.76**	**26.40**	**26.26**	**26.39**	**26.39**	**26.30**	**27.31**	**26.04**
CaO	**0.27**	**0.20**	**0.22**	**0.16**	**0.12**	**0.43**	**0.20**	**0.21**	**0.24**	**0.45**	**0.63**
SO_3	**0.78**	**0.71**	**0.76**	**0.62**	**0.60**	**0.99**	**0.71**	**0.67**	**0.78**	**0.64**	**0.75**
ThO_2	**1.66**	**2.89**	**2.57**	**3.83**	**4.38**	**2.45**	**2.83**	**2.82**	**2.88**	**2.31**	**2.75**
La_2O_3	**17.17**	**17.82**	**18.84**	**16.36**	**18.12**	**15.83**	**16.48**	**17.01**	**16.95**	**17.59**	**17.69**
Ce_2O_3	**38.95**	**37.63**	**37.22**	**36.92**	**36.96**	**38.08**	**37.85**	**37.61**	**37.61**	**37.32**	**37.25**
Pr_2O_3	**3.51**	**2.99**	**3.05**	**3.06**	**3.00**	**3.20**	**3.22**	**3.26**	**3.24**	**3.07**	**3.09**
Nd_2O_3	**10.59**	**9.90**	**10.15**	**10.76**	**9.73**	**11.16**	**10.75**	**10.31**	**10.36**	**10.66**	**10.13**
Total	**101.31**	**100.39**	**100.47**	**99.06**	**101.07**	**99.93**	**99.93**	**99.59**	**99.87**	**100.44**	**99.44**
Structural Formula Based on 4-Oxygen											
Si	**0.051**	**0.060**	**0.055**	**0.065**	**0.071**	**0.062**	**0.061**	**0.053**	**0.062**	**0.043**	**0.045**
P	**0.906**	**0.904**	**0.895**	**0.892**	**0.893**	**0.891**	**0.899**	**0.904**	**0.896**	**0.920**	**0.897**
Ca	**0.011**	**0.008**	**0.009**	**0.007**	**0.005**	**0.018**	**0.009**	**0.009**	**0.010**	**0.019**	**0.028**
S	**0.023**	**0.021**	**0.023**	**0.019**	**0.018**	**0.030**	**0.021**	**0.020**	**0.023**	**0.019**	**0.023**
Th	**0.015**	**0.026**	**0.023**	**0.036**	**0.040**	**0.022**	**0.026**	**0.026**	**0.026**	**0.021**	**0.025**
La	**0.250**	**0.262**	**0.279**	**0.247**	**0.267**	**0.234**	**0.245**	**0.254**	**0.252**	**0.258**	**0.266**
Ce	**0.564**	**0.550**	**0.548**	**0.553**	**0.541**	**0.559**	**0.558**	**0.557**	**0.554**	**0.543**	**0.555**
Pr	**0.050**	**0.044**	**0.045**	**0.046**	**0.044**	**0.047**	**0.047**	**0.048**	**0.047**	**0.045**	**0.046**
Nd	**0.150**	**0.141**	**0.146**	**0.157**	**0.139**	**0.160**	**0.155**	**0.149**	**0.149**	**0.151**	**0.147**
Cation Sum	**2.021**	**2.017**	**2.024**	**2.022**	**2.018**	**2.021**	**2.020**	**2.020**	**2.020**	**2.019**	**2.032**
(Y+REE)	**1.014**	**0.997**	**1.018**	**1.003**	**0.991**	**0.999**	**1.004**	**1.008**	**1.002**	**0.997**	**1.014**
Th+Si+Ca	**0.078**	**0.094**	**0.088**	**0.108**	**0.116**	**0.102**	**0.095**	**0.088**	**0.098**	**0.083**	**0.098**
REE+P	**1.920**	**1.901**	**1.913**	**1.895**	**1.884**	**1.889**	**1.903**	**1.912**	**1.898**	**1.917**	**1.911**
Th+Si	**0.066**	**0.086**	**0.079**	**0.100**	**0.111**	**0.084**	**0.086**	**0.079**	**0.088**	**0.064**	**0.070**

La	**162412**	**169215**	**158823**	**154894**	**164153**	**162104**	**149391**	**180531**	**161627**	**151266**	**150078**
Ce	**310442**	**331630**	**323054**	**306336**	**335926**	**343217**	**300204**	**345149**	**316285**	**297676**	**302776**
Pr	**31729**	**34455**	**34117**	**31622**	**36241**	**37269**	**31930**	**35048**	**32885**	**30916**	**31621**
Nd	**99864**	**106571**	**108714**	**101785**	**114139**	**119728**	**102471**	**112466**	**105487**	**99215**	**100550**
Sm	**6699**	**5805**	**6724**	**7448**	**5814**	**5784**	**7983**	**4669**	**6894**	**7600**	**7575**
Eu	**849.2**	**751.6**	**854.1**	**953.9**	**732.4**	**725.3**	**1024**	**603.1**	**871.9**	**968.2**	**960.8**
Gd	**2311**	**2059**	**2356**	**2672**	**2006**	**1997**	**2842**	**1690**	**2392**	**2657**	**2669**
Tb	**109.1**	**97.3**	**110.8**	**127.2**	**96.1**	**93.9**	**135.0**	**80.3**	**113.0**	**125.7**	**121.9**
Dy	**177.5**	**170.2**	**189.9**	**217.0**	**163.7**	**156.3**	**238.9**	**139.8**	**190.0**	**219.9**	**208.7**
Ho	**13.74**	**13.58**	**15.28**	**18.14**	**13.09**	**12.70**	**19.56**	**11.26**	**15.83**	**17.42**	**16.31**
Er	**45.71**	**42.66**	**49.30**	**55.39**	**42.08**	**40.70**	**60.80**	**33.24**	**47.98**	**55.54**	**54.23**
Tm	**1.01**	**1.15**	**1.22**	**1.43**	**1.21**	**0.98**	**1.43**	**0.79**	**1.25**	**1.26**	**1.28**
Yb	**4.99**	**5.73**	**6.61**	**6.41**	**5.80**	**5.69**	**7.41**	**3.92**	**6.24**	**6.00**	**7.10**
Lu	**0.55**	**0.70**	**0.92**	**0.97**	**0.74**	**0.66**	**0.84**	**0.46**	**0.73**	**0.79**	**0.91**
Hf	**0.31**	**0.14**	**0.21**	**0.32**	**0.19**	**0.16**	**0.21**	**0.20**	**0.19**	**0.14**	**0.19**
Ta	**0.02**	**0.02**	**0.02**	**0.05**	**0.02**	**0.02**	**0.04**	**0.02**	**0.04**	**0.05**	**0.03**
Pb	**57.87**	**38.41**	**43.09**	**47.94**	**35.55**	**31.68**	**49.71**	**140.46**	**92.95**	**221.72**	**37.07**
Th	**23399**	**24216**	**23687**	**22771**	**23910**	**22873**	**22325**	**18393**	**23050**	**26218**	**18290**
U	**115.0**	**146.9**	**180.4**	**181.3**	**146.5**	**136.8**	**184.0**	**66.6**	**150.4**	**162.9**	**140.7**
Li	**6.53**	**3.71**	**7.50**	**5.67**	**4.34**	**2.46**	**5.78**	**5.90**	**8.32**	**6.89**	**4.78**
B	**1.28**	**2.21**	**1.41**	**1.44**	**1.60**	**0.82**	**1.39**	**1.25**	**2.54**	**1.23**	**1.03**
Sc	**0.00**	**0.32**	**0.18**	**0.18**	**0.00**	**0.16**	**0.89**	**0.00**	**0.11**	**0.00**	**0.24**
V	**26.82**	**19.22**	**20.23**	**24.04**	**19.06**	**17.21**	**23.93**	**17.56**	**22.19**	**24.81**	**28.35**
Cr	**2.88**	**0.00**	**0.96**	**9.56**	**1.93**	**1.18**	**5.61**	**0.30**	**12.43**	**13.16**	**0.49**
Ga	**650.6**	**534.2**	**598.6**	**696.3**	**520.4**	**499.4**	**732.0**	**452.8**	**632.6**	**709.7**	**731.4**
Ge	**1089**	**912.9**	**1040**	**1159**	**902.2**	**868.0**	**1222**	**753.7**	**1093**	**1213**	**1217**
Sr	**405.1**	**551.2**	**635.9**	**667.6**	**727.1**	**539.5**	**667.3**	**396.1**	**613.5**	**559.2**	**702.0**
Y	**310.0**	**314.8**	**341.7**	**398.3**	**300.2**	**281.5**	**427.3**	**247.4**	**350.6**	**389.8**	**370.4**
Zr	**0.57**	**0.42**	**0.30**	**0.59**	**0.26**	**0.26**	**0.31**	**0.43**	**0.53**	**0.73**	**0.60**
Nb	**0.25**	**0.11**	**0.11**	**0.14**	**0.10**	**0.10**	**0.13**	**0.10**	**0.52**	**0.15**	**0.12**
Mo	**0.26**	**0.28**	**0.13**	**0.29**	**0.20**	**0.22**	**0.20**	**0.11**	**0.25**	**0.33**	**0.03**
Sn	**0.18**	**0.16**	**0.09**	**0.01**	**0.01**	**0.04**	**0.12**	**0.02**	**0.07**	**0.15**	**0.01**

Ba	**2.84**	**0.81**	**1.16**	**1.12**	**0.90**	**0.84**	**0.72**	**2.15**	**2.88**	**2.57**	**1.47**

715

716

717

718

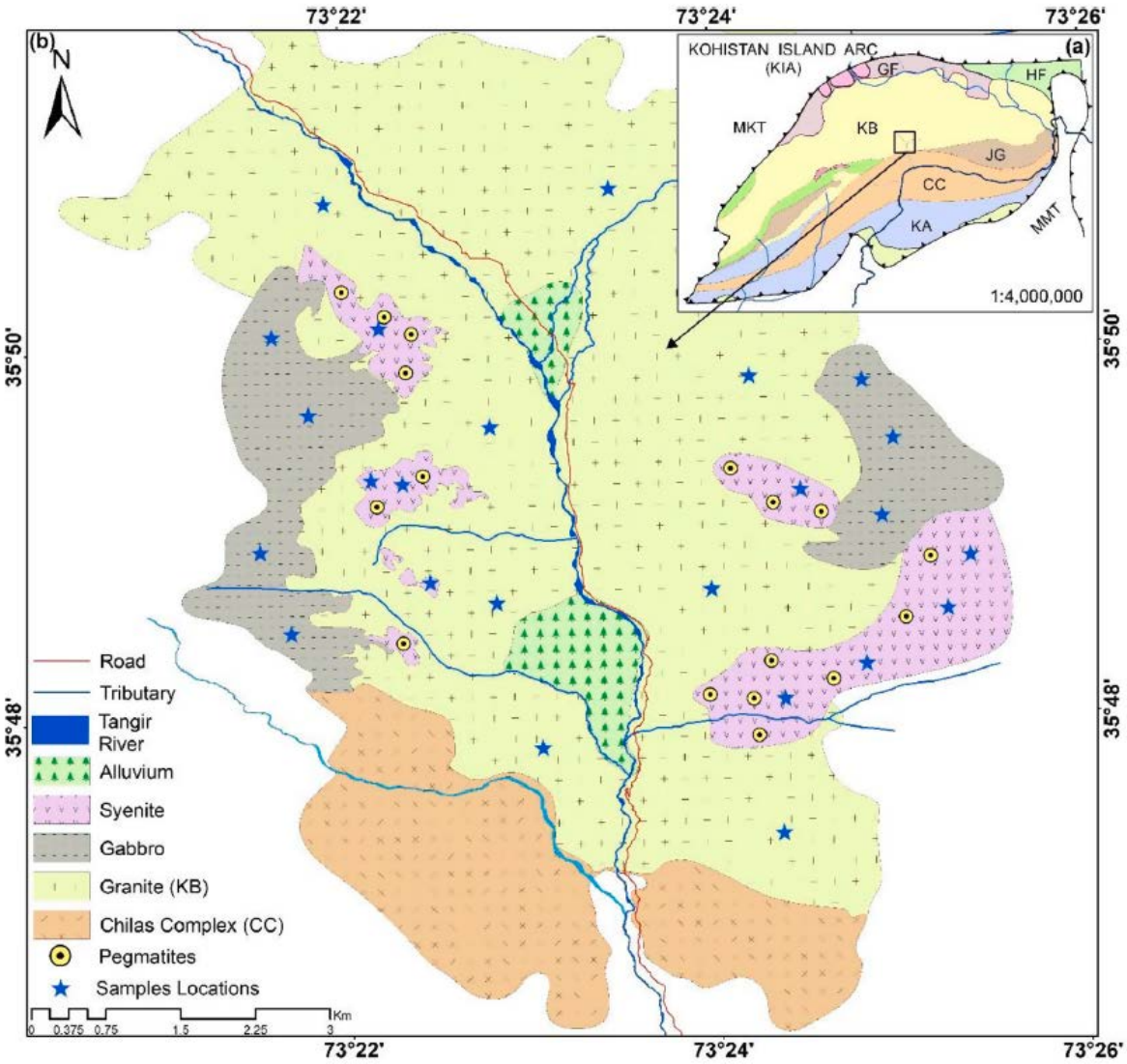

Fig. 1. (a) Simplified geological map of the Kohistan Island Arc, North Pakistan, showing the location of the study area (after Treloar et al., 1996); (b) Geological map showing the distribution of the syenite and the REE-bearing pegmatite in the Kohistan Batholith.

Fig. 2. Field and hand specimen photographs of the syenite and the pegmatite. (a) A fresh porphyritic syenite; (b) A pegmatite vein hosted by the syenite; (c–e) Multidirectional pegmatitic veins showing sharp contact with the host syenite; (f) A lenticular pegmatitic patch hosted in the syenite; (g) Chevkinite crystals disseminated in the pegmatite; (h) Chevkinite crystals from the pegmatite; (i) Alkali amphibole associated with a perthite phenocryst in the pegmatite. Aeg-aegirine, Rct-richterite, Prth-perthite, Chv-chevkinite.

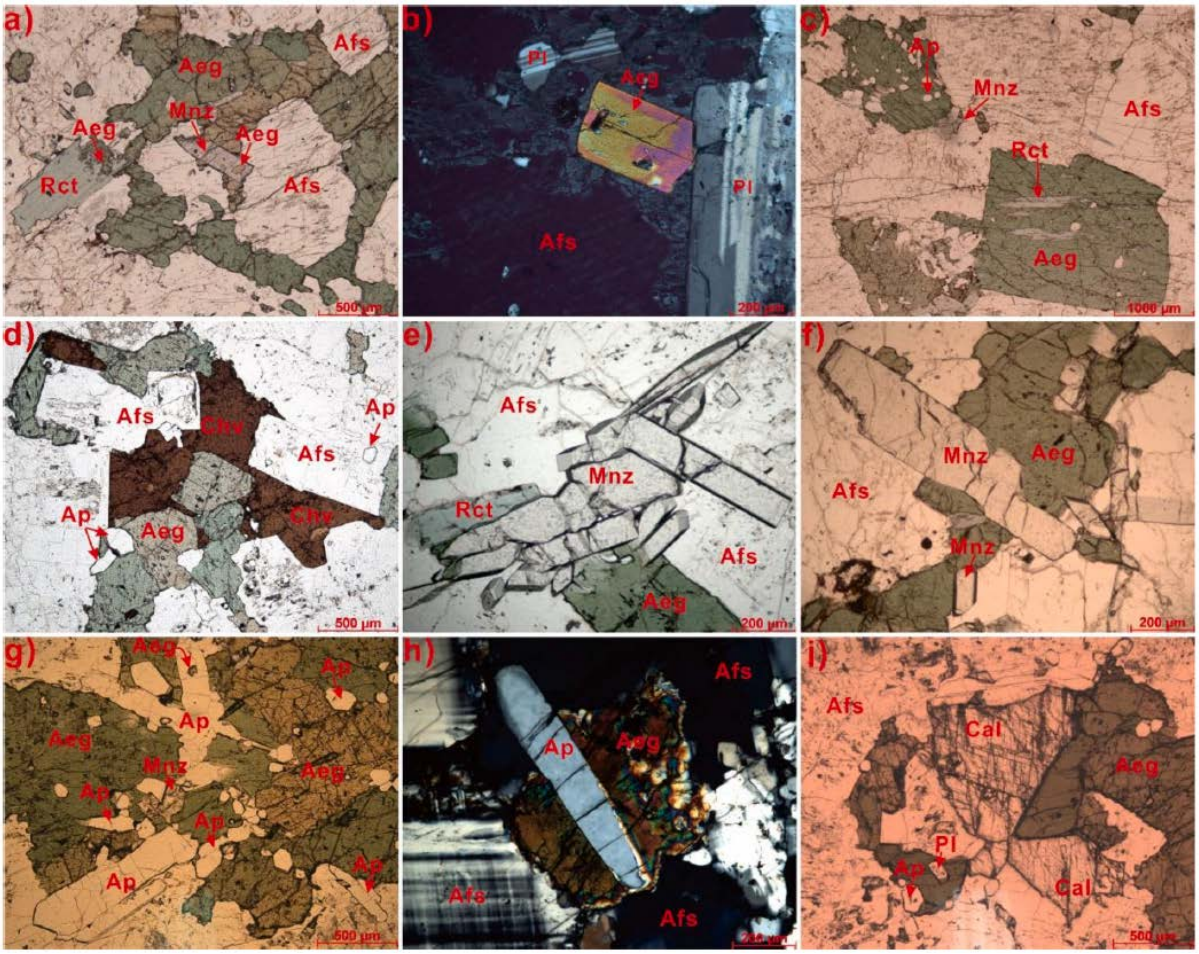

Fig. 3. Microphotographs of the syenite. (a) Aegirine and richterite interstitial to early formed alkali feldspar, showing agpaitic-like crystallization sequence; (b) Euhedral early-formed aegirine and plagioclase; (c) Richterite formed at the expense of aegirine along cleavage planes; (d) Anhedral chevkinite crystals interstitial to both mafic and felsic silicates; (e) Monazite cluster closely associated with aegirine and richterite; (f–h) Monazite grains showing cross-cutting relationship to aegirine; (i) Calcite grains interstitial to mafic and felsic minerals. Aeg-aegirine, Rct-richterite, Afs-alkaline feldspars, Mnz-monazite, Pl-plagioclase, Ap-apatite, Chvchevkinite, Mnz-monazite, Cal-calcite.

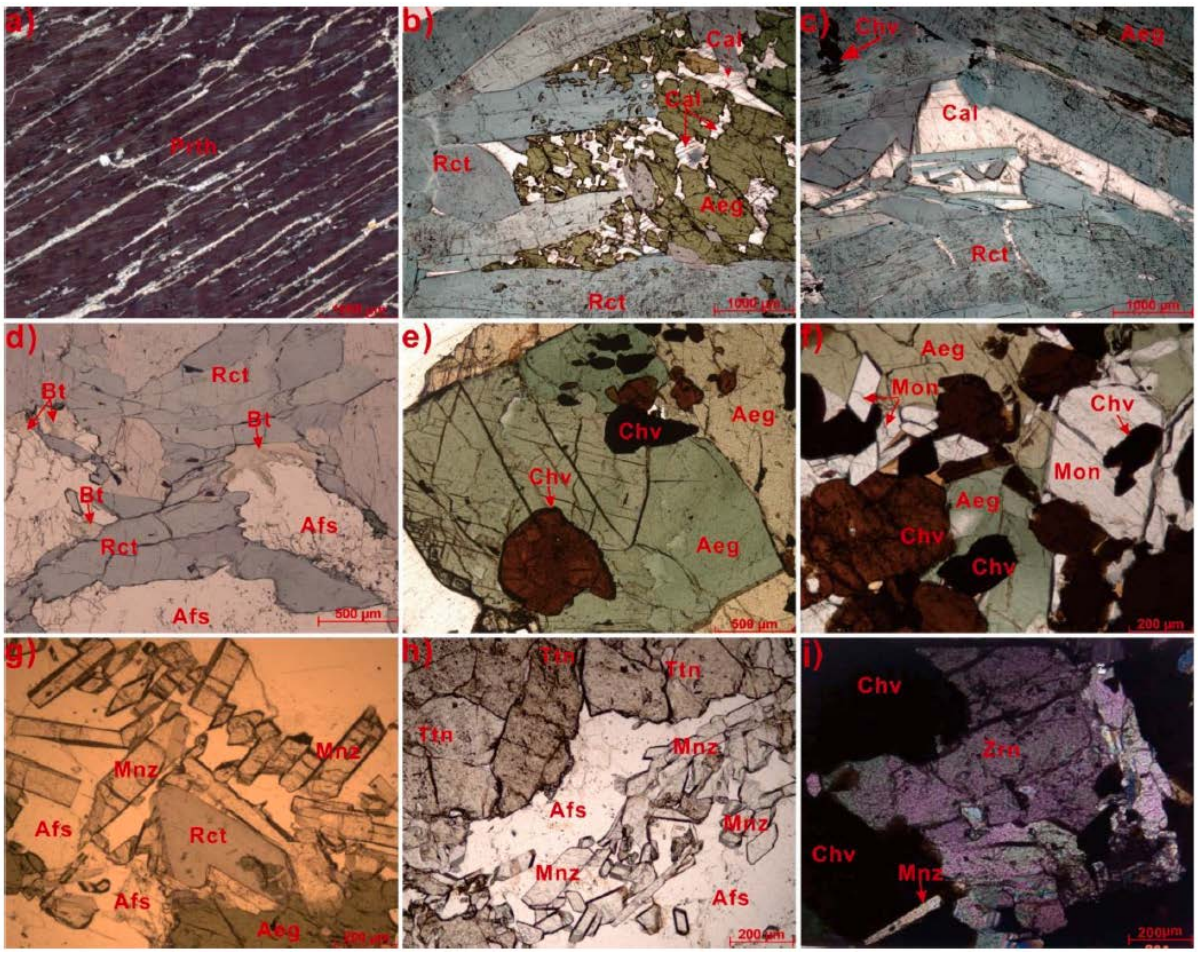

Fig. 4. Microphotographs of the pegmatite. (a) Perthite in the pegmatite showing regular intergrowth of sodic blebs; (b,c) Calcite interstitial to the aegirine and richterite grains; (d) Biotite flakes interstitial to the richterite and alkaline feldspar grains; (e) Aegirine phenocryst poikilitically enclosing chevkinite crystals; (f) Chevkinite associated with monazite and aegirine; (g) Monazite cluster associated with richterite, aegirine and alkaline feldspar; (h) Titanite clusters associated with monazite clusters; (i) Zircon in the pegmatite associated with chevkinite. Prth-Perthite, Rct-richterite, Aeg-aegirine, Cal-calcite, Chv-chevkinite, Mnz-monazite, Ttn-titanite, Zrn-zircon.

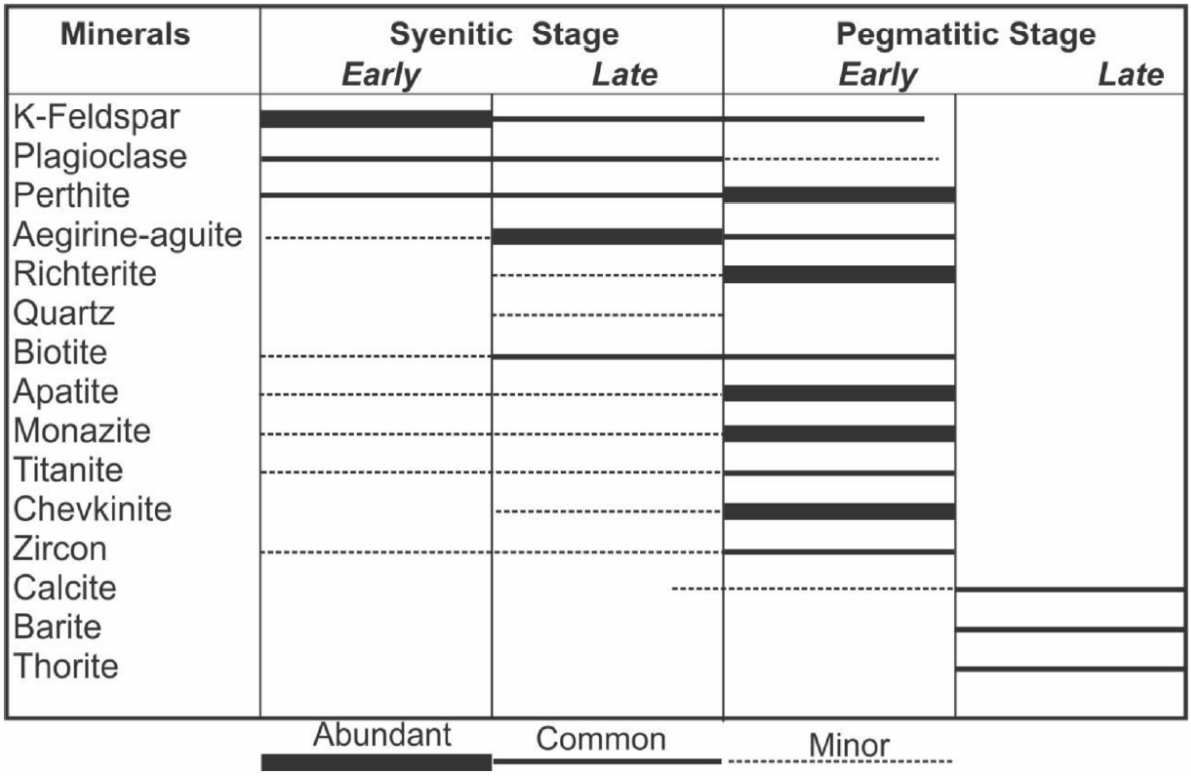

Fig. 5. Mineral paragenetic sequence in the syenite and the pegmatite.

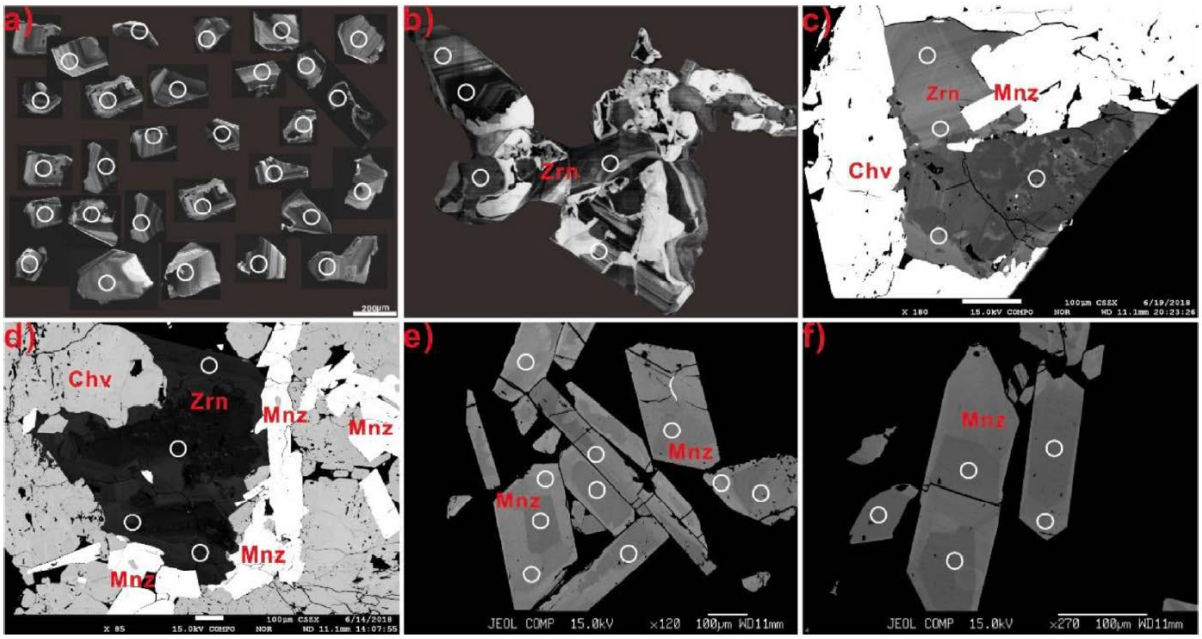

Fig. 6. (a) Cathodoluminescence (CL) images of representative zircon crystals from the syenite showing clear magmatic zoning; (b) CL images of zircon from the pegmatite showing subtle magmatic zoning; (c,d) Back-scatter electron (BSE) images of zircons in the pegmatite showing subtle magmatic zoning; (e-f) BSE images of monazites in the pegmatite showing clear magmatic sector zonings. Zrn-zircon, Mnz-monazite, Chv-chevkinite.

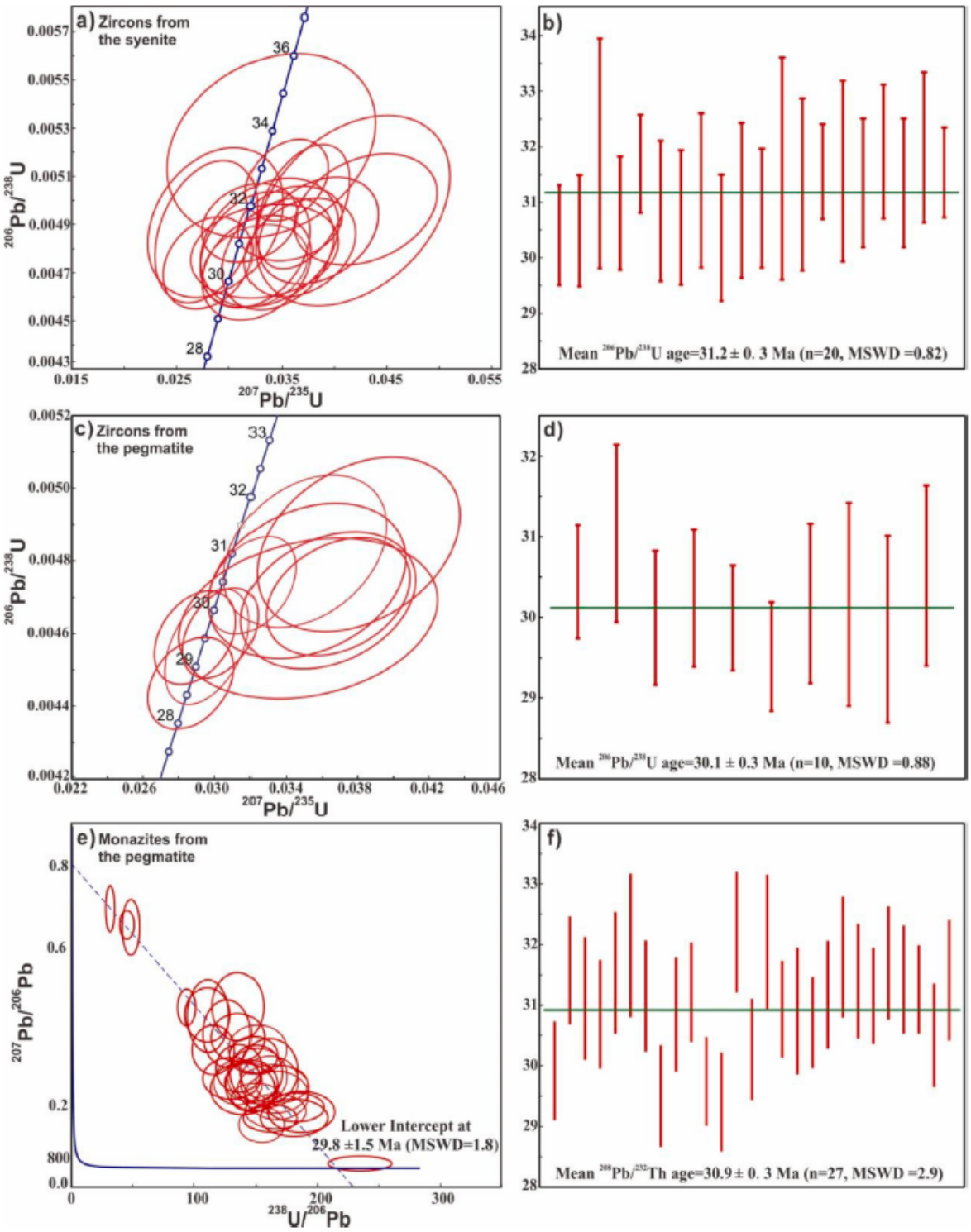

Fig. 7. LA-ICP-MS zircon and monazite U-Th-Pb age concordia diagrams and weighted mean ages. (a-b) zircons from the syenite; (c,d) zircons from the pegmatite; (e,f) monazites from the pegmatite.

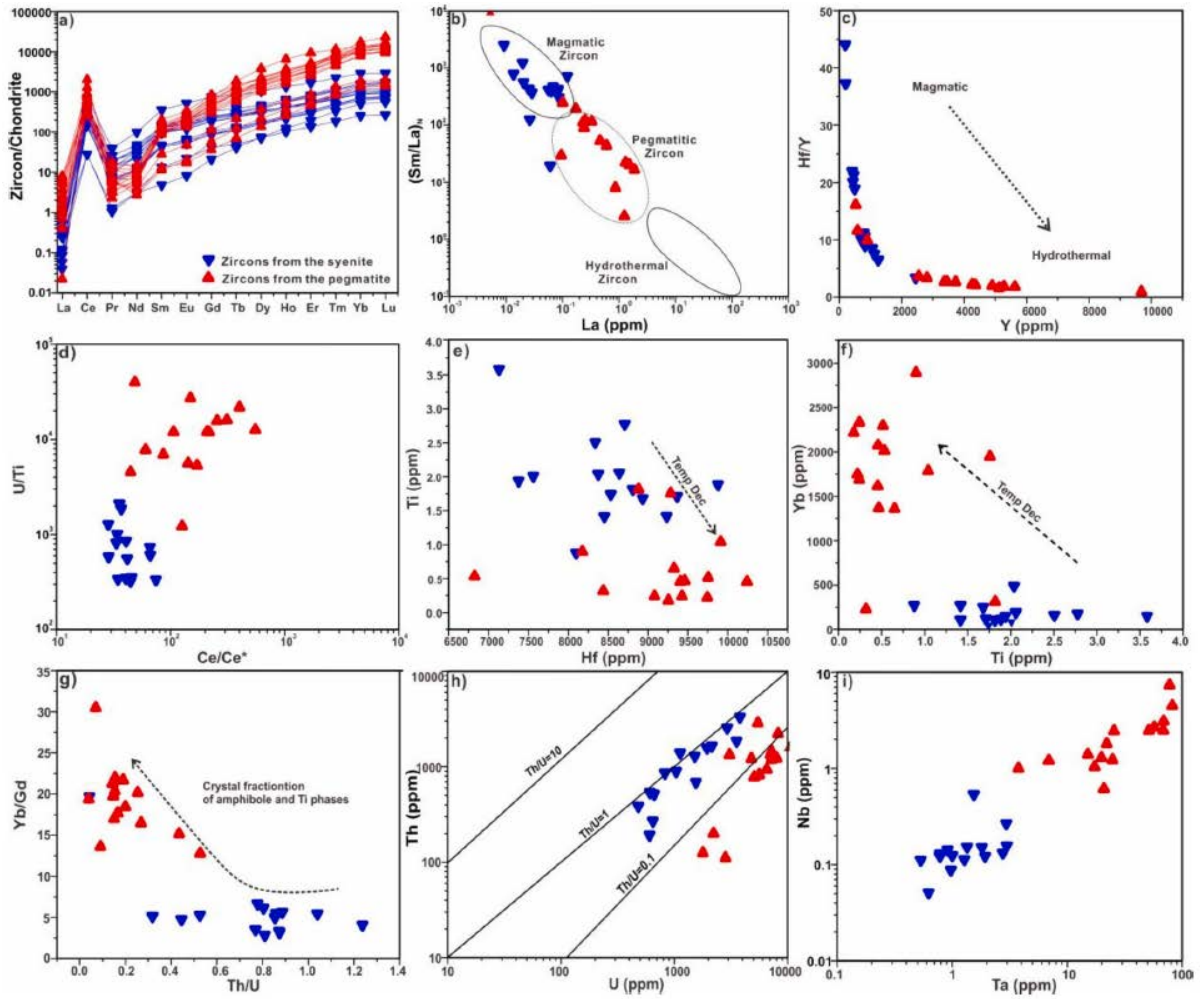

Fig. 8. (a) Chondrite-normalized REE patterns of zircons from the syenite and the pegmatite; (b) zircon discrimination diagram of (Sm/La)N vs. La (after Hoskin, 2005); (c) Y vs. Hf/Y, (d) Ce/Ce* vs. U/Ti, (e) Hf vs. Ti, (f) Ti vs. Yb, (g) Th/U vs. Yb/Gd, (h) U vs. Th, (i) Nb vs. Ta plots of zircons from the syenite and the pegmatite.

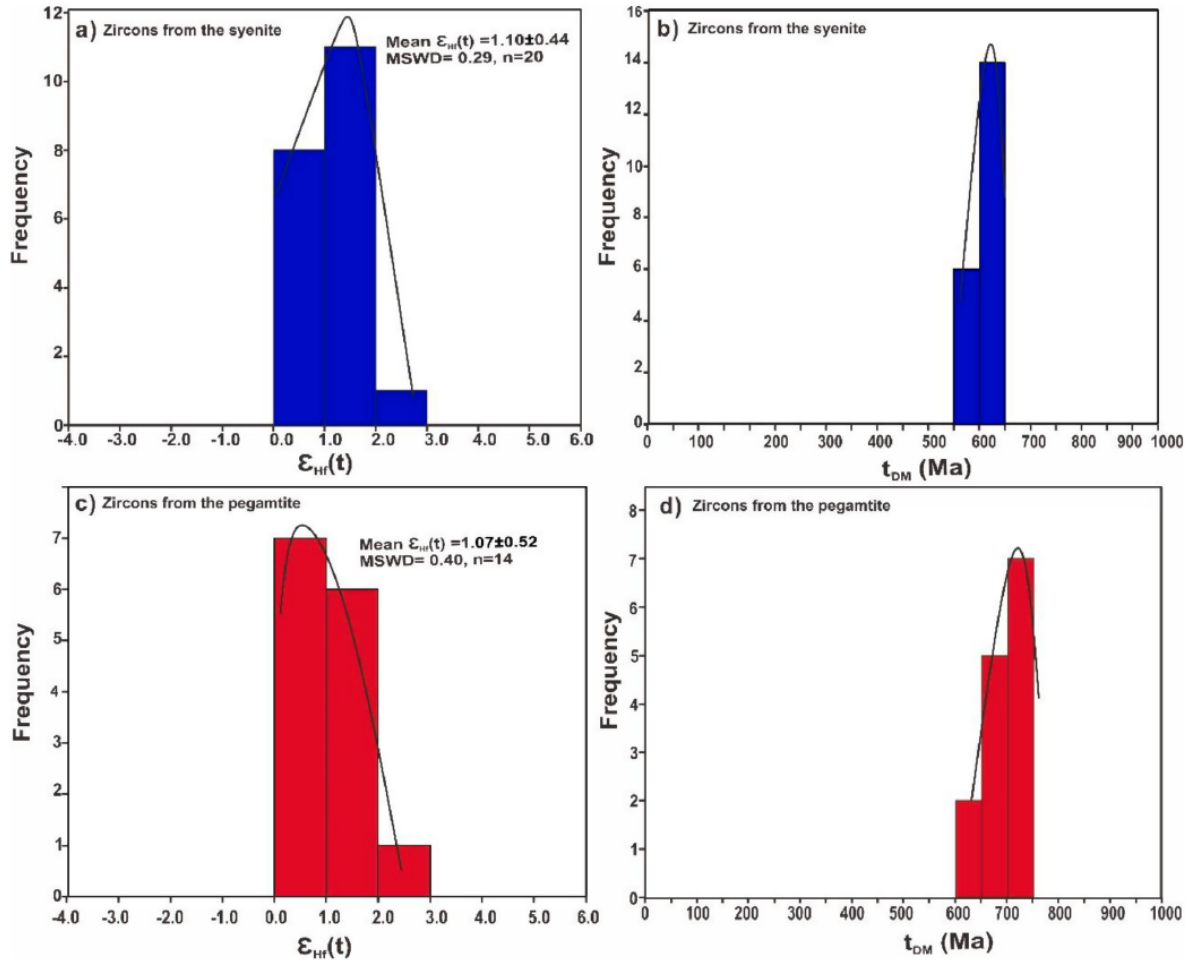

Fig. 9. Histograms of εHf (t) values and Hf model ages of zircons from the syenite (a-b) and the pegmatite (c,d).

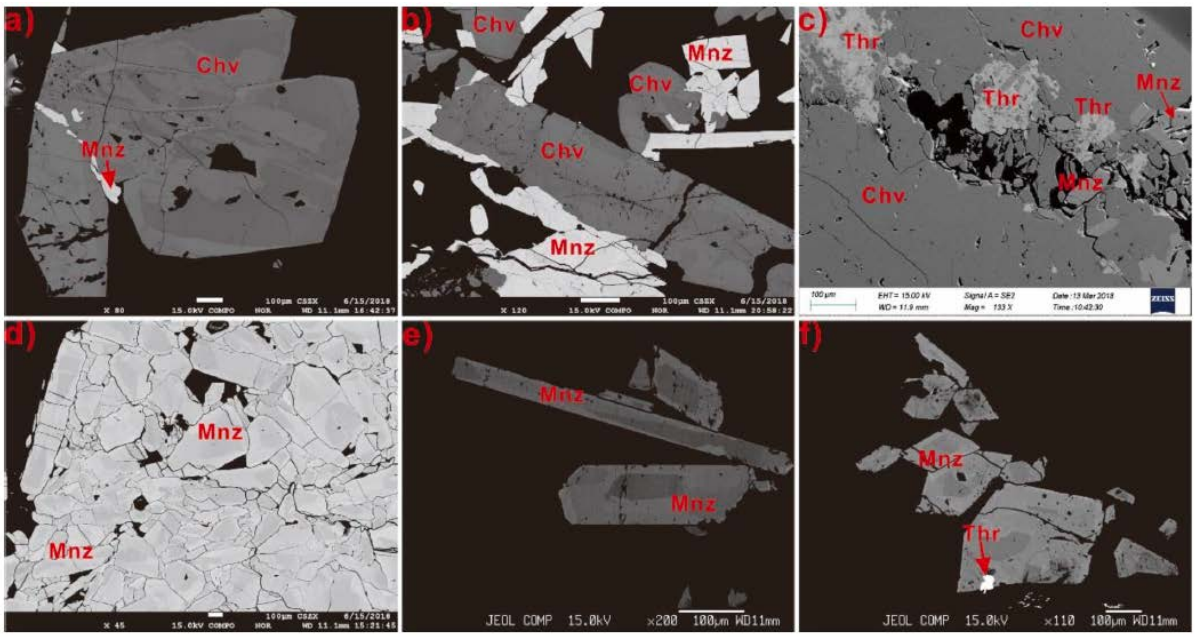

Fig. 10. BSE images of chevkinites and monazites in the pegmatite. (a) Complex patchy zoning in chevkinites; (b) Chevkinite phenocryst and monazite cluster; (c) Intimate association of anhedral thorite with chevkinite; (d–f) Monazite clusters showing obvious sector zoning.

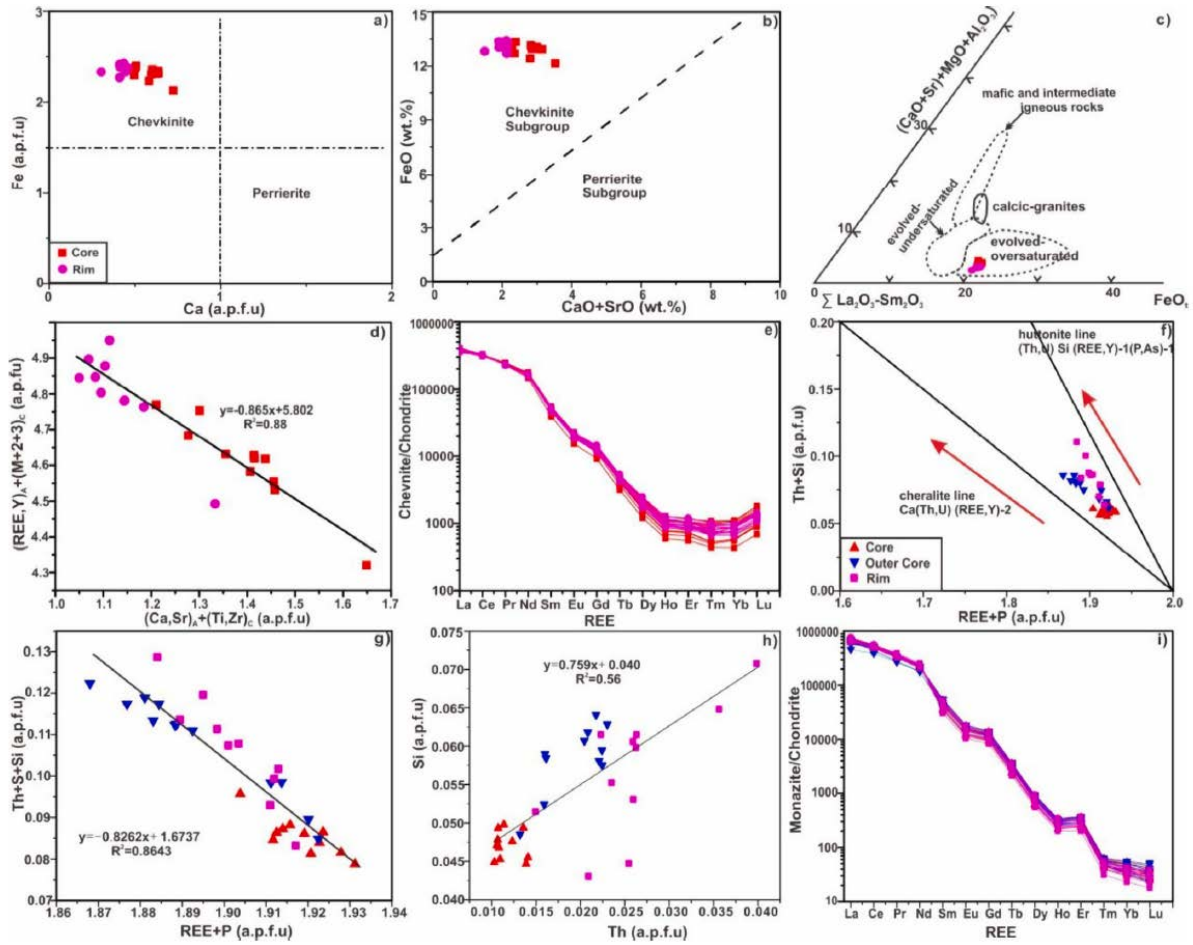

Fig. 11. (a–b) Discrimination plots for chevkinite and perrierite minerals of the chevkinite-group (after Macdonald and Belkin, 2002); (c) Ternary plot for chevkinite group minerals from different rock types (after Macdonald and Belkin, 2002); (d) Cations substitutions of chevkinite; (e) Chondrite-normalized REE patterns of chevkinite; (f–h) Substitution diagrams of Th + Si vs. REE + P, Th + S + Si vs. REE + P, and Th vs. Si of monazite; (i) Chondrite-normalized REE patterns of monazite.

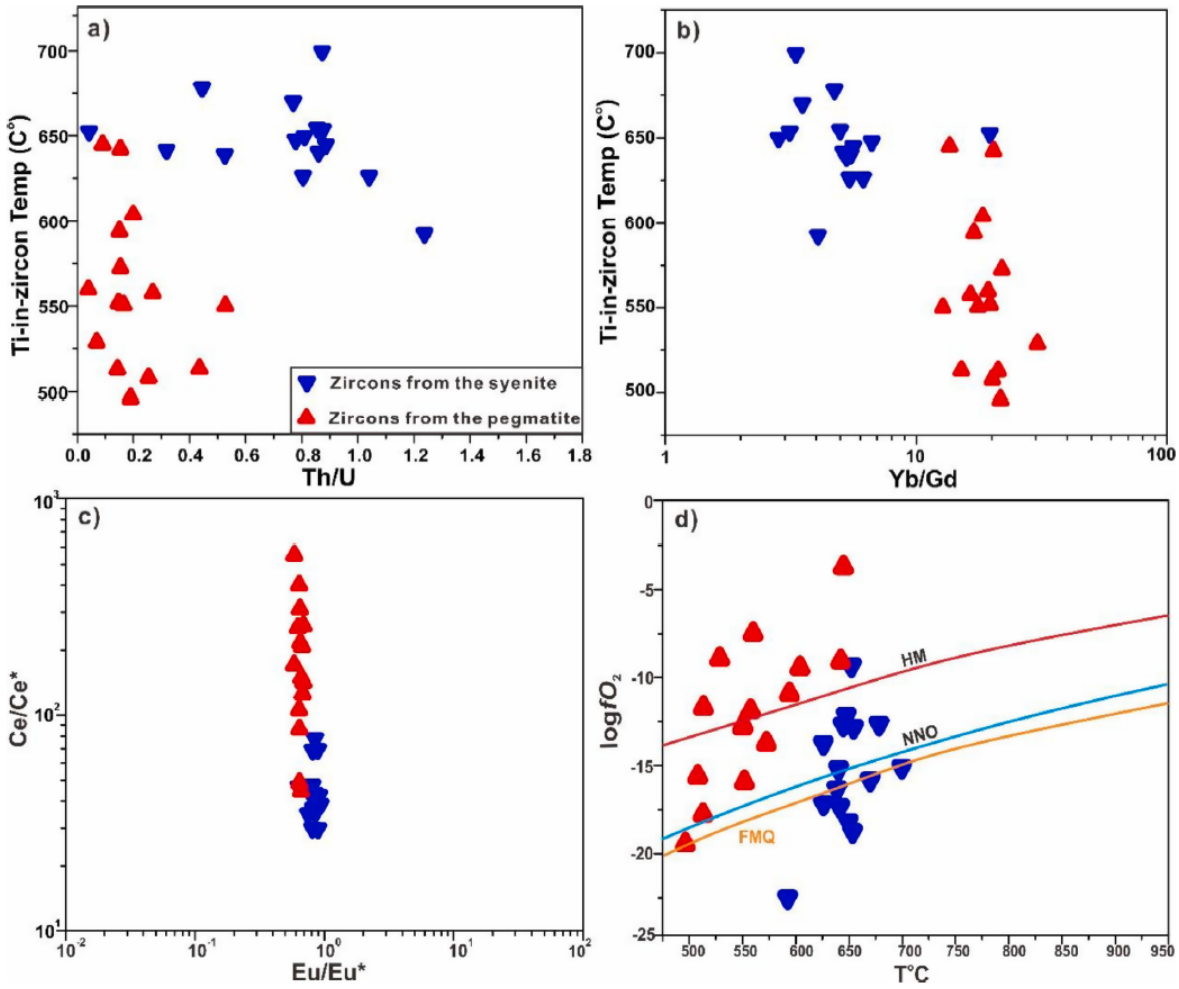

Fig. 12. (a,b) Ti-in-zircon temperatures vs. Th/U and Yb/Gd of zircons from the syenite and the pegmatite; (c) Eu/Eu* vs. Ce/Ce* of zircons; (d) Zircon temperatures vs. log fO_2 calculated after Li et al. (2019).